Fingerprints of quantum spin ice in Raman scattering

Jianlong Fu,[1] Jeffrey G. Rau,[2] Michel J. P. Gingras,[2,3] and Natalia B. Perkins[1]
[1]*School of Physics and Astronomy, University of Minnesota, Minneapolis, Minnesota 55116, USA*
[2]*Department of Physics and Astronomy, University of Waterloo, Waterloo, ON, N2L 3G1, Canada*
[3]*Canadian Institute for Advanced Research, 180 Dundas St. W., Toronto, ON, M5G 1Z8, Canada*
(Received 7 April 2017; published 19 July 2017)

We develop a theory of the dynamical response of a minimal model of quantum spin ice (QSI) by means of inelastic light scattering. In particular, we are interested in the Raman response of the fractionalized U(1) spin liquid realized in the XXZ QSI. We show that the low-energy Raman intensity is dominated by spinon and gauge fluctuations. We find that the Raman response in the QSI state of that model appears only in the T_{2g} polarization channel. We show that the Raman intensity profile displays a broad continuum from the spinons and coupled spinon and gauge fluctuations, and a low-energy peak arising entirely from gauge fluctuations. Both features originate from the exotic interaction between photon and the fractionalized excitations of QSI. Our theoretical results suggest that inelastic Raman scattering can in principle serve as a promising experimental probe of the nature of a U(1) spin liquid in QSI.

DOI: 10.1103/PhysRevB.96.035136

I. INTRODUCTION

Quantum spin liquids (QSLs) have proven to be one of the most fascinating and challenging subjects in modern condensed matter physics [1–5]. They are known to host a remarkable set of emergent phenomena, including long-range entanglement, topological ground-state degeneracy, and a number of unusual fractionalized excitations such as fermionic or bosonic spinons as well as emergent gauge excitations. In recent years, there has been significant progress both in the theoretical understanding of such phenomena and in identifying realistic microscopic models that may host QSL phases. Notable examples include the spin-1/2 Heisenberg antiferromagnet on the kagome lattice [6–10], the family of exactly solvable Kitaev-type models [11–13], and quantum spin ice [4,14–24].

Direct experimental observation and characterization of QSLs is challenging. Unlike states with spontaneously broken symmetries, the topological order characteristic of QSLs [5] cannot be captured by a local order parameter and thus cannot be directly detected by local measurements. Identifying QSLs thus requires finding experimental probes that provide information without relying on the measurement of local order parameters. One of the most promising avenues in this direction is the characterization of the excitations of QSL candidates. The fractionalized excitations of a QSL can be probed by conventional methods such as inelastic neutron scattering [25], Raman scattering [26–30] or resonant x-ray scattering (RIXS) [31–33], all offering signatures that enable their detection. Due to their fractionalized nature, these kinds of scattering probes necessarily create multiparticle excitations in the system. The appearance of such multiparticle continua in their dynamical response is a hallmark of QSL behavior [34–39]. These continua are in stark contrast with the excitation spectra of conventionally ordered phases, where sharp single-particle excitations are expected. Given the field currently still lacks the experimental methods to probe the topological order of QSLs, it is therefore important to have both a qualitative and a quantitative understanding of these multiparticle continua and how they manifest themselves in various experimental scattering probes and in QSL candidates.

In this paper, we study such a dynamical response in a model QSL, quantum spin ice (QSI). Defined on the pyrochlore lattice, a network of corner-sharing tetrahedra (see Fig. 1), this QSL emerges naturally from the classical spin ice limit [3,4,40]. In this limit, there are a macroscopic number of ground states characterized by the so-called "ice rule"; each tetrahedron must be in a two-in/two-out state [40]. Excitations about this manifold have three spins up and one down (or vice-versa) and can be separated at no energy cost [41]. As first shown by Hermele *et al.* [14], adding transverse exchange induces quantum tunneling between different ice states. A sufficiently weak tunneling stabilizes a QSL ground state with an emergent U(1) gauge field and bosonic spinon excitations [4,14,19–21]. Much effort has been put forth to understand the nature of the QSI phase as well as its static and dynamic properties [14,17–21,42–46].

These theoretical studies have sparked intense experimental activity aiming to find a concrete realization of QSI. The wide range of rare-earth pyrochlore materials [4,47] have provided an ample playground for this search. Potential candidates for hosting a QSI phase currently include $Tb_2Ti_2O_7$, $Yb_2Ti_2O_7$, the $Pr_2M_2O_7$ family ($M = Zr$, Sn, Hf) as well as the canonical classical spin ices $Dy_2Ti_2O_7$ and $Ho_2Ti_2O_7$ (see Ref. [4] for a survey). However, the physics of these materials is complex; for many, it is even unclear how close they are to the classical spin ice limit. Identifying experimental probes that are sensitive to both the gauge and spinon excitations that manifest in QSI would thus be useful for a better characterization of these QSI candidates. Perhaps more importantly, it would deepen our general understanding of the dynamical response of QSLs and their various excitations.

In this paper, we propose that inelastic Raman scattering may be of particular interest for QSI systems. In a loose sense, we are inspired by rather recent works on Raman scattering in Kitaev QSLs [26–30]. Using photons as a probe, the Raman response can in principle offer insights on the excitation spectrum of a QSI that may not be accessible through usual methods such as inelastic neutron scattering. Below, we derive

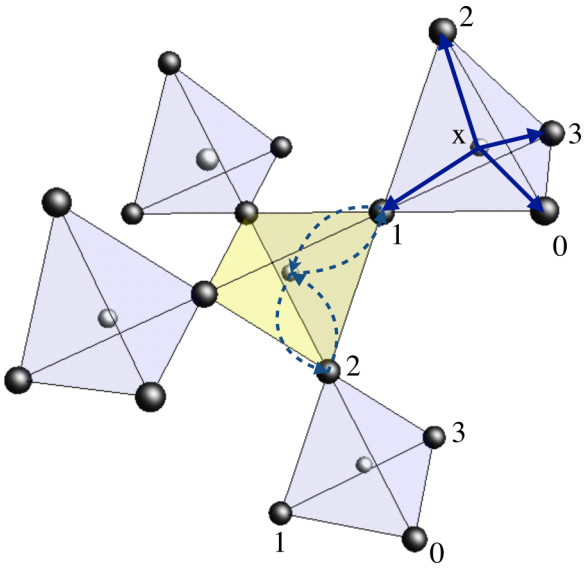

FIG. 1. The pyrochlore lattice relevant for QSI materials. The centers of blue and yellow tetrahedra, labeled by $\boldsymbol{x}$, form the $\langle A\rangle$ and $\langle B\rangle$ sublattices of the diamond lattice, correspondingly. $\mu = 0,1,2,3$ label the bonds of the diamond lattice. The spins $S_{\boldsymbol{x},\mu}$ reside on the pyrochlore sites located on the middle of the bond μ. The dashed lines illustrate the electron hopping paths involved in the superexchange processes that generate the Raman vertex.

the Raman vertex for relevant rare-earth pyrochlore materials using the traditional framework of an effective Hamiltonian for the interaction of light with spin degrees of freedom [26,48–50]. Applying these results to an effective theory of QSI, we show how the gapped and deconfined spinons as well as emergent gapless gauge modes appear in the Raman spectrum. Intriguingly, we find that real light can scatter from the emergent "light" of QSI [17] and produce a measurable response. In addition, the spinon excitations themselves have a direct signature in the Raman spectrum.

The structure of the paper is as follows. In Secs. II–IV, we set our notations and review the basic concepts of QSI and its elementary excitations [14,17–19,21]. In Sec. V, we briefly review the Loudon-Fleury theory of Raman scattering in Mott insulators needed for our study. Armed with this, we then derive the relevant Raman operator involving the superexchange processes between pseudospins that represent the magnetic degrees of freedom. By studying the polarization dependence of the Raman response, we explicitly show that the response occurs only in the T_{2g} polarization channel. In Sec. VI, we compute the Raman response for the XXZ QSI. In particular, we first separate three contributions to the Raman response—from pure spinon excitations, from gauge fluctuations and from their hybridization—and then present the numerical results for the total Raman intensity in the T_{2g} channel. Some discussion and a conclusion are given in Secs. VII and VIII, respectively.

II. SPIN HAMILTONIAN

Before delving into the details of the Raman process, we first review the relevant anisotropic exchange models for the pertinent pyrochlore materials. In the current materials of interest, which may realize QSI, the magnetic degrees of freedom originate from rare-earth ions [4]. Although we are not per se confining ourselves to the details of the rare-earth ions that currently form the majority of the QSI materials, it is useful to set the stage and make some general observations about the spin Hamiltonian so far considered in the theoretical and experimental investigations of QSI systems [4].

In rare-earth ions, the atomic interactions dominate; the free-ion ground state is determined by following Hund's rules, first minimizing the Coulomb energy, followed by the spin-orbit energy. These free-ion states have well defined total angular momentum J and (approximately) well-defined total orbital and spin angular momenta. In a crystalline environment, due to the electric fields from the surrounding ions, the remaining $2J+1$ degeneracy of this manifold is partially lifted. When J is a half-odd-integer, only Kramers' degeneracy remains and one has a series of doublets for the relevant D_{3d} site symmetry [47]. With respect to this symmetry, these can transform either like spin-1/2 objects, a "pseudospin" doublet (as in $Yb_2Ti_2O_7$ or $Er_2Ti_2O_7$) [18], or like a more exotic "dipolar-octupolar" doublet [51] (as in $Dy_2Ti_2O_7$ and $Nd_2Zr_2O_7$). For integer J, Kramers' theorem does not apply and singlet states are possible. However, the D_{3d} site symmetry can allow a nonmagnetic doublet, a so-called non-Kramers doublet (as, for example, in $Ho_2Ti_2O_7$ or $Tb_2Ti_2O_7$) [47]. If well separated from the other crystal field levels, each of these kinds of crystal field doublets behaves like an effective spin-1/2 degree of freedom. For this reason, we will refer to all of these states as a "spin" regardless of whether they are pseudo-spin-1/2, dipolar-octupolar or non-Kramers type.

To describe these doublets, we introduce the spin operators $\boldsymbol{S}_i$, defined in the local basis at each site [18]. For the dipolar-octupolar and non-Kramers doublets, only S_i^z contributes to the magnetic dipole moment with $\boldsymbol{\mu}_i = -g\mu_B S_i^z \hat{\boldsymbol{z}}_i$, where $\hat{\boldsymbol{z}}_i$ is the local [111] direction. For the pseudo-spin-1/2 case, both the $\hat{\boldsymbol{z}}_i$ component and the components perpendicular to $\hat{\boldsymbol{z}}_i$ contribute to the dipole moment. Since these three types of doublets transform quite differently under lattice symmetries [20,51], the allowed exchange interactions are generally distinct. The most general nearest-neighbor anisotropic exchange model on the pyrochlore lattice can be written as [18,19]

$$\begin{aligned} H_{\rm ex} = \sum_{\langle ij\rangle} \big[& J_{zz} S_i^z S_j^z - J_{\pm}(S_i^+ S_j^- + S_i^- S_j^+) \\ & + J_{\pm\pm}(\gamma_{ij} S_i^+ S_j^+ + \text{H.c.}) \\ & + J_{z\pm}\big(\zeta_{ij}\big[S_i^z S_j^+ + S_i^+ S_j^z\big] + \text{H.c.}\big)\big], \end{aligned} \tag{1}$$

where the matrices $\zeta_{ij} = -\gamma_{ij}^*$ and γ_{ij} are defined in Appendix A. For the case of a pseudo-spin-1/2 doublet, all of these couplings are allowed. For a non-Kramers doublet, one has $J_{z\pm} = 0$ whereas for a dipolar-octupolar doublet, the phases are absent, i.e., $\gamma_{ij} = 1$ and $\zeta_{ij} = 1$ [51]. Microscopically, these kinds of short-range anisotropic interactions can be generated by various superexchange mechanisms [16,22]. If $J_{zz} > 0$ and $J_{\pm\pm} = J_{\pm} = J_{z\pm} = 0$, one recovers classical spin

ice.[1] Introducing a finite $J_\pm$ or $J_{\pm\pm}$ with $J_{zz} \gg J_\pm, J_{\pm\pm} \gg J_{z\pm}$ induces quantum tunneling between the ice states [14,19] and stabilizes [17,42–44] a QSI ground state.[2] While in $Dy_2Ti_2O_7$ and $Ho_2Ti_2O_7$ one expects $J_\pm$ and $J_{\pm\pm}$ to be negligible [22], in other materials such as $Yb_2Ti_2O_7$, $Er_2Ti_2O_7$, or $Tb_2Ti_2O_7$, experiments strongly suggests that these couplings are significant [18,52–55]. Since we are interested in the spin ice limit, we shall restrict ourselves to cases where J_{zz} is dominant and is antiferromagnetic ($J_{zz} > 0$). In the remainder of the paper, we thus work with the dimensionless ratios

$$j_\pm = J_\pm/J_{zz}, \quad j_{z\pm} = J_{z\pm}/J_{zz}, \quad j_{\pm\pm} = J_{\pm\pm}/J_{zz}, \tag{2}$$

which we assume to be small such that we remain in the QSI phase [19,20].

III. QUANTUM SPIN ICE

We now review the slave-particle description of QSI [19], using the formulation introduced in Ref. [21]. In the following, we use the notation of Refs. [19,21] and label the pyrochlore sites by a combined index $(\boldsymbol{x},\mu)$, in which $\boldsymbol{x}$ denotes a diamond lattice site (center of a tetrahedron) belonging to sublattice $\langle A\rangle$ and $\mu = 0,1,2,3$ are the four nearest neighbors of the diamond site, as shown in Fig. 1. The spin at the center of the bond $\langle \boldsymbol{x},\boldsymbol{x}+\boldsymbol{\mu}\rangle$ is then labeled as $\boldsymbol{S}_{\boldsymbol{x},\mu}$, with $\boldsymbol{\mu}$ being the vector connecting the two neighboring diamond sites shown in Fig. 1.

We study the exchange Hamiltonian, Eq. (1), in an enlarged Hilbert space containing both the charge and the spin degrees of freedom separately. We construct this by introducing a new Hilbert space for the charge operator $Q_{\boldsymbol{x}}$ on the diamond lattice sites independent of the spins on the pyrochlore sites. In terms of the spins, the charges are defined as

$$Q_{\boldsymbol{x}} = \begin{cases} +\sum_\mu S^z_{\boldsymbol{x},\mu}, & \boldsymbol{x} \in \langle A\rangle, \\ -\sum_\mu S^z_{\boldsymbol{x}-\hat{\boldsymbol{\mu}},\mu}, & \boldsymbol{x} \in \langle B\rangle. \end{cases} \tag{3}$$

The charge operator $Q_{\boldsymbol{x}}$ characterizes violations of the ice rules: $Q_{\boldsymbol{x}} = 0$ being satisfied for a two-in/two-out state, while tetrahedra with three-in/one-out or three-out/one-in have $Q_{\boldsymbol{x}} = \pm 1$ and those with all-in/all-out have $Q_{\boldsymbol{x}} = \pm 2$.

Next, we enlarge the range of allowed charges from strictly $0, \pm 1$, and ± 2 to include all integers. Explicitly, if we define the physical Hilbert space as $\mathcal{H}_{\text{phys}} = \bigotimes_{\boldsymbol{x},\mu} \mathcal{H}_{1/2}$, where $\mathcal{H}_{1/2}$ is the spin Hilbert space, then the extended space is

$$\mathcal{H}_{\text{ext}} = \left[\bigotimes_{\boldsymbol{x},\mu} \mathcal{H}_{1/2}\right] \otimes \left[\bigotimes_{\boldsymbol{x}} \mathcal{H}_{O(2)}\right] \equiv \mathcal{H}_s \otimes \mathcal{H}_Q, \tag{4}$$

and where $\mathcal{H}_{O(2)}$ is the Hilbert space of an $O(2)$ rotor, defined at each diamond site and spanned by an infinite set of basis states that satisfy $Q_{\boldsymbol{x}}\,|q_{\boldsymbol{x}}\rangle = q_{\boldsymbol{x}}\,|q_{\boldsymbol{x}}\rangle$, where $q_{\boldsymbol{x}}$ is an integer. We define the physical subspace as the one in which the $Q_{\boldsymbol{x}}$ operators satisfy the constraint of Eq. (3).

In this extended space, one then introduces a phase $\theta_{\boldsymbol{x}}$, conjugate to the charge operators $Q_{\boldsymbol{x}}$ [19]. These two operators satisfy the canonical commutation relation

$$[\theta_{\boldsymbol{x}}, Q_{\boldsymbol{x}'}] = i\delta_{\boldsymbol{x},\boldsymbol{x}'}. \tag{5}$$

The quantization of $Q_{\boldsymbol{x}}$ implies the periodicity of $\theta_{\boldsymbol{x}}$. The operators $Q_{\boldsymbol{x}}$ and $\theta_{\boldsymbol{x}}$ allow us to introduce a spinon operator $\psi_{\boldsymbol{x}}$, which is the basic element in a slave particle description of spin ice. To be precise, we define the raising and lowering operators $\psi^\dagger_{\boldsymbol{x}} = e^{+i\theta_x}$ and $\psi_{\boldsymbol{x}} = e^{-i\theta_x}$, satisfying

$$[\psi^\dagger_{\boldsymbol{x}}, Q_{\boldsymbol{x}'}] = -\psi^\dagger_{\boldsymbol{x}}\delta_{\boldsymbol{x},\boldsymbol{x}'}, \tag{6a}$$

$$[\psi_{\boldsymbol{x}}, Q_{\boldsymbol{x}'}] = +\psi_{\boldsymbol{x}}\delta_{\boldsymbol{x},\boldsymbol{x}'}, \tag{6b}$$

which thus increase or decrease the charge quantum number at diamond lattice site $\boldsymbol{x}$. We then interpret $Q_{\boldsymbol{x}}$ as the spinon number operator in the quantum theory, with $\psi^\dagger_{\boldsymbol{x}}$ and $\psi_{\boldsymbol{x}}$ being spinon creation and annihilation operators [19], which live in the Hilbert space $\mathcal{H}_Q$.

For the $\mathcal{H}_s$ part of the extended Hilbert space, we define *new* auxiliary spin-1/2 operators, $\boldsymbol{s}_{\boldsymbol{x},\mu}$. The original physical spin-1/2 operators $\boldsymbol{S}_{\boldsymbol{x},\mu}$ can be expressed in terms of the $\boldsymbol{s}_{\boldsymbol{x},\mu}$, $\psi^\dagger_{\boldsymbol{x}}$ and $\psi_{\boldsymbol{x}}$ operators as

$$S^+_{\boldsymbol{x},\mu} = \psi^\dagger_{\boldsymbol{x}} s^+_{\boldsymbol{x},\mu}\psi_{\boldsymbol{x}+\hat{\boldsymbol{\mu}}}, \tag{7a}$$

$$S^-_{\boldsymbol{x},\mu} = \psi^\dagger_{\boldsymbol{x}+\hat{\boldsymbol{\mu}}} s^-_{\boldsymbol{x},\mu}\psi_{\boldsymbol{x}}, \tag{7b}$$

$$S^z_{\boldsymbol{x},\mu} = s^z_{\boldsymbol{x},\mu}. \tag{7c}$$

These combinations of operators are chosen such that the canonical commutation relations of the original spin-1/2 operators $\boldsymbol{S}_{\boldsymbol{x},\mu}$ are preserved, and the physical constraint defined by Eq. (3) is also respected. If we were able to enforce these constraints exactly, Eqs. (3)–(7) would then constitute an exact reformulation of the original spin-1/2 problem of Eq. (1). While such an exact description is not feasible, this set of variables have nevertheless proven [19,21] to be a useful starting point for describing the QSI phases of the anisotropic exchange model given in Eq. (1).

The enlargement of the Hilbert space implies a large degree of redundancy in this description. In particular, note that the mapping defined by Eq. (7) is invariant under the U(1) transformation

$$\psi_{\boldsymbol{x}} \to \psi_{\boldsymbol{x}} e^{i\alpha_{\boldsymbol{x}}}, \quad s^\pm_{\boldsymbol{x},\mu} \to s^\pm_{\boldsymbol{x},\mu} e^{\pm i(\alpha_{\boldsymbol{x}} - \alpha_{\boldsymbol{x}+\hat{\boldsymbol{\mu}}})}, \tag{8}$$

for an arbitrary local phase $\alpha_{\boldsymbol{x}}$. This gauge redundancy can be made explicit by recasting the $\boldsymbol{s}_{\boldsymbol{x},\mu}$ operators in terms of an emergent gauge field $A_{\boldsymbol{x},\mu}$ and an emergent electric field $E_{\boldsymbol{x},\mu}$ via

$$s^\pm_{\boldsymbol{x},\mu} = |s^\pm_{\boldsymbol{x},\mu}| e^{\pm i A_{\boldsymbol{x},\mu}}, \quad s^z_{\boldsymbol{x},\mu} = E_{\boldsymbol{x},\mu}. \tag{9}$$

[1] We are focusing on a nearest-neighbor description and exclude long-range dipolar interactions.

[2] Note that finite $J_{z\pm}$, for a pseudo-spin-1/2 doublet, produces an ordered ferromagnetic state drawn from the ice manifold [19]. To obtain QSI, one can thus only include $J_{z\pm}$ in concert with $J_\pm$ or $J_{\pm\pm}$. For a dipolar-octupolar doublet, $J_{z\pm}$ is entirely innocuous and can be removed by a local redefinition of the doublet states.

To simplify the problem, we replace the transverse components of the spin operator by their average value, with $|s^{\pm}_{\boldsymbol{x},\mu}| \approx \langle |s^{\pm}_{\boldsymbol{x},\mu}| \rangle$, and only keep the phase of $s^{\pm}_{\boldsymbol{x},\mu}$ as dynamical variable [2]. It is easy to check that the electric field and the gauge field satisfy the commutation relation

$$[A_{\boldsymbol{x},\mu}, E_{\boldsymbol{x}',\nu}] = i\delta_{\boldsymbol{x}\boldsymbol{x}'}\delta_{\mu\nu}. \tag{10}$$

By construction, these fields are compact given the redundancy built into the definition of $A_{\boldsymbol{x},\mu}$ and the periodicity of $\theta_{\boldsymbol{x}}$. This kind of mapping of an auxiliary spin-1/2 system to a gauge theory has been explored in many contexts; we refer the reader to the literature for further details [14,17,46].

Having performed this reformulation of the original spin degrees of freedom, we now rewrite $H_{\rm ex}$ in terms of these new variables. One finds

$$\begin{aligned} H_{\rm ex} = {} & \frac{1}{2}\sum_{\boldsymbol{x}} Q^2_{\boldsymbol{x}} - j_{\pm}\langle s^{\pm}\rangle^2 \sum_{\boldsymbol{x}\in\langle A\rangle}\sum_{\mu<\nu}[\psi^{\dagger}_{\boldsymbol{x}} e^{i(A_{\boldsymbol{x},\mu}-A_{\boldsymbol{x}+\hat{\boldsymbol{\mu}}-\hat{\boldsymbol{\nu}},\nu})}\psi_{\boldsymbol{x}+\hat{\boldsymbol{\mu}}-\hat{\boldsymbol{\nu}}} + \psi^{\dagger}_{\boldsymbol{x}+\hat{\boldsymbol{\mu}}} e^{-i(A_{\boldsymbol{x},\mu}-A_{\boldsymbol{x},\nu})}\psi_{\boldsymbol{x}+\hat{\boldsymbol{\nu}}} + \text{H.c.}] \\ & - j_{z\pm}\langle s^{\pm}\rangle \sum_{\boldsymbol{x}\in\langle A\rangle}\sum_{\mu\neq\nu}[E_{\boldsymbol{x},\mu}(\psi^{\dagger}_{\boldsymbol{x}} e^{iA_{\boldsymbol{x},\nu}}\psi_{\boldsymbol{x}+\hat{\boldsymbol{\nu}}} + \psi^{\dagger}_{\boldsymbol{x}+\hat{\boldsymbol{\mu}}-\hat{\boldsymbol{\nu}}} e^{iA_{\boldsymbol{x}+\hat{\boldsymbol{\mu}}-\hat{\boldsymbol{\nu}},\nu}}\psi_{\boldsymbol{x}+\hat{\boldsymbol{\mu}}})\zeta_{\mu\nu} + \text{H.c.}] \\ & - j_{\pm\pm}\langle s^{\pm}\rangle^2 \sum_{\boldsymbol{x}\in\langle A\rangle}\sum_{\mu<\nu}[(\psi^{\dagger}_{\boldsymbol{x}}\psi_{\boldsymbol{x}+\hat{\boldsymbol{\mu}}}\psi^{\dagger}_{\boldsymbol{x}}\psi_{\boldsymbol{x}+\hat{\boldsymbol{\nu}}} + \psi^{\dagger}_{\boldsymbol{x}+\hat{\boldsymbol{\mu}}-\hat{\boldsymbol{\nu}}}\psi_{\boldsymbol{x}+\hat{\boldsymbol{\mu}}}\psi^{\dagger}_{\boldsymbol{x}}\psi_{\boldsymbol{x}+\hat{\boldsymbol{\mu}}})\gamma_{\mu\nu} + \text{H.c.}]. \end{aligned} \tag{11}$$

Here we see that the J_{zz} and $J_{\pm}$ parts of $H_{\rm ex}$ describe the spinon degrees of freedom, as well as their interaction with the gauge field A. Including finite $J_{z\pm}$ introduces further spinon-gauge couplings, while $J_{\pm\pm}$ produces direct four-spinon interactions. In the current work, we consider only $J_{z\pm} = J_{\pm\pm} = 0$. Focusing on this limit has several advantages; aside from being theoretically simpler, this limit is shared among the exchange models for all three types of microscopic degrees of freedom discussed in Sec. II.[3]

As it stands, the reformulated model $H_{\rm ex}$ of Eq. (11) lacks any dynamics for the gauge fields at leading order. To remedy this, we follow Ref. [21] and add to the model

$$H_g \equiv \frac{U}{2}\sum_{\boldsymbol{x}\in\langle A\rangle,\mu} E^2_{\boldsymbol{x},\mu} - g\sum_{\hexagon}\cos\left(\sum_{\boldsymbol{x}\mu\in\hexagon} A_{\boldsymbol{x},\mu}\right), \tag{12}$$

to endow the gauge sector with its own dynamics. We denote the full model,[4] with this additional gauge part, as

$$H_{\rm QSI} \equiv H_{\rm ex} + H_g. \tag{13}$$

This final form is inspired from the effective Hamiltonian that arises when considering the effects of transverse exchange on the ground-state spin-ice manifold [14]. The "ring"-exchange term, proportional to g in Eq. (12), appears first at third order in $j_{\pm}$ or at sixth order in $j_{\pm\pm}$ [14]. This effective model has been analyzed in detail in Refs. [14], [17]. Here we have added it by hand to make up for some of the deficiencies in the slave-particle approach. In terms of $A_{\boldsymbol{x}\mu}$, this second term describes the "lattice curl" of the gauge field, while the first term penalizes large electric fields, as required for the mapping of the auxiliary spin-1/2 spins, $\boldsymbol{s}_{\boldsymbol{x}\mu}$, to a gauge theory. For our purposes, we will assume the compactness of the gauge field is innocuous; namely the effects of the gauge monopoles [14,56] are not considered. Consistent with this assumption, we also take $A_{\boldsymbol{x},\mu} \ll 1$. Under this condition, H_g can be expanded to give [17,21]

$$H_g = \sum_{\boldsymbol{x}\in\langle A\rangle,\mu}\left(\frac{U}{2}E^2_{\boldsymbol{x},\mu} + \frac{g}{2}B^2_{\boldsymbol{x},\mu}\right), \tag{14}$$

where the magnetic fluxes $B_{\boldsymbol{x},\mu}$ derive from the lattice curl of the gauge field [17] $A_{\boldsymbol{x},\mu}$. In such a phenomenological description, the magnitudes of U and g must be set by comparison with more precise calculations within the full model. For the case of $j_{\pm\pm} = j_{z\pm} = 0$ they have been estimated [17,21] to be on the order of $\sim j^3_{\pm}$. More specifically, we use the values of Ref. [21], given as

$$g \simeq 24 j^3_{\pm}, \quad U \simeq 2.16 j^3_{\pm}. \tag{15}$$

IV. SPINON DYNAMICS AND GAUGE FLUCTUATIONS

We now consider the physics of $H_{\rm QSI}$ [Eq. (13)] in the XXZ limit, where $j_{\pm\pm} = j_{z\pm} = 0$. To simplify the spinon-gauge coupling, we first expand in $A_{\boldsymbol{x}\mu}$, considering only the leading

[3] In addition, since there is no sign problem for the exchange model when $J_{\pm} > 0$ and $J_{\pm\pm} = J_{z\pm} = 0$. This would in principle allow validation of these results though direct numerical simulation [42,44]. However, given the difficulty and opacity of such calculations, here we pursue a more analytical route.

[4] One should also include the constraint of Eq. (3) in addition to the Hamiltonian. This can be implemented by including a nondynamical constraint field $\phi_{\boldsymbol{x}}$ into the problem [21]. This induces a Coulomb interaction between the charges $Q_{\boldsymbol{x}}$ on different sites. Within low-density limit of the exclusive boson representation (to be introduced) these terms can be neglected.

terms in the expansion of $e^{iA_{x,\mu}}$. Defining $\tilde{j}_\pm = j_\pm \langle s^\pm \rangle^2$, we can write

$$H_{\rm QSI} \sim \left[\frac{1}{2} \sum_{\boldsymbol{x}} Q_{\boldsymbol{x}}^2 - \tilde{j}_\pm \sum_{\boldsymbol{x} \in \langle A \rangle} \sum_{\mu<\nu} (\psi_{\boldsymbol{x}}^\dagger \psi_{\boldsymbol{x}+\hat{\boldsymbol{\mu}}-\hat{\boldsymbol{\nu}}} + \psi_{\boldsymbol{x}+\hat{\boldsymbol{\mu}}}^\dagger \psi_{\boldsymbol{x}+\hat{\boldsymbol{\nu}}} + \text{H.c.}) \right]$$
$$- \left[\tilde{j}_\pm \sum_{\boldsymbol{x} \in \langle A \rangle} \sum_{\mu<\nu} i(\psi_{\boldsymbol{x}}^\dagger \psi_{\boldsymbol{x}+\hat{\boldsymbol{\mu}}-\hat{\boldsymbol{\nu}}} - \psi_{\boldsymbol{x}} \psi_{\boldsymbol{x}+\hat{\boldsymbol{\mu}}-\hat{\boldsymbol{\nu}}}^\dagger)(A_{\boldsymbol{x},\mu} - A_{\boldsymbol{x}+\boldsymbol{\mu}-\boldsymbol{\nu},\nu}) + i(\psi_{\boldsymbol{x}+\hat{\boldsymbol{\mu}}}^\dagger \psi_{\boldsymbol{x}+\hat{\boldsymbol{\nu}}} - \psi_{\boldsymbol{x}+\hat{\boldsymbol{\nu}}}^\dagger \psi_{\boldsymbol{x}+\hat{\boldsymbol{\mu}}})(A_{\boldsymbol{x},\nu} - A_{\boldsymbol{x},\mu}) \right] + H_g$$
$$\equiv H_\psi + H_{\psi A} + H_g. \tag{16}$$

We have broken this Hamiltonian into three parts: H_ψ, which describes the kinetic energy of the bosonic spinons $\psi_{\boldsymbol{x}}$ and their "charging" energy $\sim Q_{\boldsymbol{x}}^2$, and $H_{\psi A}$, which describes a minimal coupling between the spinons and the emergent U(1) gauge field.

The spinon part, H_ψ, defines a quantum rotor model and is thus difficult to solve even on its own. This can be written as

$$H_\psi = \frac{1}{2} \sum_{\boldsymbol{x}} Q_{\boldsymbol{x}}^2 - \tilde{j}_\pm \times \sum_{\boldsymbol{x} \in \langle A \rangle} \sum_{\mu<\nu} (\psi_{\boldsymbol{x}}^\dagger \psi_{\boldsymbol{x}+\hat{\boldsymbol{\mu}}-\hat{\boldsymbol{\nu}}} + \psi_{\boldsymbol{x}+\hat{\boldsymbol{\mu}}}^\dagger \psi_{\boldsymbol{x}+\hat{\boldsymbol{\nu}}} + \text{H.c.}),$$
$$= \frac{1}{2} \sum_{\boldsymbol{x}} Q_{\boldsymbol{x}}^2 - \tilde{j}_\pm \sum_{\mu<\nu} \sum_{\boldsymbol{k}\lambda} f_{\mu\nu}^\psi(\boldsymbol{k}) \psi_{\boldsymbol{k}\lambda}^\dagger \psi_{\boldsymbol{k}\lambda}, \tag{17}$$

where we have introduced the sublattice label $\lambda = \langle A \rangle, \langle B \rangle$ and defined the vertex

$$f_{\mu\nu}^\psi(\boldsymbol{k}) \equiv 2 \cos[\boldsymbol{k} \cdot (\boldsymbol{\mu} - \boldsymbol{\nu})]. \tag{18}$$

To approximately solve this rotor model, we use the "exclusive boson" representation introduced in Ref. [21]:

$$\psi_{\boldsymbol{x}} = \frac{d_{\boldsymbol{x}} + b_{\boldsymbol{x}}^\dagger}{(1 + d_{\boldsymbol{x}}^\dagger d_{\boldsymbol{x}} + b_{\boldsymbol{x}}^\dagger b_{\boldsymbol{x}})^{1/2}}, \tag{19a}$$
$$Q_{\boldsymbol{x}} = d_{\boldsymbol{x}}^\dagger d_{\boldsymbol{x}} - b_{\boldsymbol{x}}^\dagger b_{\boldsymbol{x}}. \tag{19b}$$

Here, $b_{\boldsymbol{x}}$ and $d_{\boldsymbol{x}}$ are bosonic operators constrained to satisfy $b_{\boldsymbol{x}} d_{\boldsymbol{x}} \equiv b_{\boldsymbol{x}}^\dagger d_{\boldsymbol{x}}^\dagger \equiv 0$ for all the basis states. Under the approximation that the density of bosons is small, and thus dropping all four-boson terms, the Hamiltonian H_ψ is simplified significantly into a quadratic form. This can then be diagonalized with the help of a Bogoliubov transformation, giving

$$H_\psi = \sum_{\boldsymbol{k}\lambda} E_{\boldsymbol{k}} (\tilde{d}_{\boldsymbol{k}\lambda}^\dagger \tilde{d}_{\boldsymbol{k}\lambda} + \tilde{b}_{\boldsymbol{k}\lambda}^\dagger \tilde{b}_{\boldsymbol{k}\lambda}) + \text{const.}, \tag{20}$$

where $\tilde{b}_{\boldsymbol{k}\lambda}$, $\tilde{d}_{\boldsymbol{k}\lambda}$ are the Bogoliubov quasiparticles and the dispersion relation $E_{\boldsymbol{k}}$ is given by

$$E_{\boldsymbol{k}} = \frac{1}{2} \left[1 - 2\tilde{j}_\pm \sum_{\alpha \neq \beta} \cos\left(\frac{k_\alpha}{2}\right) \cos\left(\frac{k_\beta}{2}\right) \right]^{1/2}, \tag{21}$$

where $\alpha, \beta = x, y, z$ are the three global cubic directions. Explicit expressions for the relationship between the spinons $\psi_{\boldsymbol{k}\lambda}$ and the bosons $\tilde{b}_{\boldsymbol{k}\lambda}$, $\tilde{d}_{\boldsymbol{k}\lambda}$ are given in Ref. [21]. The Green's function for the spinon field [21] is then given by

$$G_\psi(\omega, \boldsymbol{k}) = \int dt\, e^{i\omega t} [-i \langle \mathcal{T} \psi_{\boldsymbol{k}}(t) \psi_{\boldsymbol{k}'}^\dagger(0) \rangle],$$
$$= \frac{1}{2E_{\boldsymbol{k}}} \left(\frac{1}{\omega - E_{\boldsymbol{k}} + i\delta} - \frac{1}{\omega + E_{\boldsymbol{k}} - i\delta} \right), \tag{22}$$

where $\mathcal{T}$ implements time ordering and $\delta = 0^+$.

Next, we discuss the dynamics of the gauge Hamiltonian, H_g. This can be done using standard methods [21] once the condition $A_{\boldsymbol{x},\mu} \ll 1$ has been imposed. Explicitly, one has

$$H_g \sim \frac{U}{2} \sum_{\boldsymbol{x} \in \langle A \rangle, \mu} E_{\boldsymbol{x},\mu}^2 + \frac{g}{2} \sum_{\hexagon} \left(\sum_{\boldsymbol{x}\mu \in \hexagon} A_{\boldsymbol{x},\mu} \right)^2. \tag{23}$$

To diagonalize H_g, a linear transformation is defined as

$$A_{\boldsymbol{p},\mu} = \sum_{\gamma=0,1} \eta_{\mu\gamma}(\boldsymbol{p}) a_{\gamma,\boldsymbol{p}}, \quad E_{\boldsymbol{p},\mu} = \sum_{\gamma=0,1} \eta_{\mu\gamma}(\boldsymbol{p}) e_{\gamma,\boldsymbol{p}}, \tag{24}$$

where $\eta_{\mu\gamma}(\boldsymbol{p})$ is a matrix satisfying

$$\eta_{\mu\gamma}(-\boldsymbol{p}) = \eta_{\mu\gamma}^*(\boldsymbol{p}),$$
$$\sum_\gamma \eta_{\mu\gamma}(\boldsymbol{p}) \eta_{\nu\gamma}(-\boldsymbol{p}) = \sum_\gamma \eta_{\mu\gamma}(\boldsymbol{p}) \eta_{\nu\gamma}^*(\boldsymbol{p}) = \delta_{\mu\nu}. \tag{25}$$

The two operators, $a_{\gamma,\boldsymbol{p}}$ and $e_{\gamma',\boldsymbol{p}}$, satisfy the canonical commutation relation $[a_{\gamma,\boldsymbol{p}}, e_{\gamma',\boldsymbol{p}'}] = i\delta_{\boldsymbol{p},\boldsymbol{p}'}\delta_{\gamma,\gamma'}$. This way, the a excitations act like positions and e excitations act like momenta in a quantum harmonic oscillator. This unitary transformation diagonalizes H_g, resulting in

$$H_g = \sum_{\boldsymbol{p}\gamma} \left[\frac{U}{2} e_{\gamma,\boldsymbol{p}} e_{\gamma,-\boldsymbol{p}} + \frac{\epsilon_{\boldsymbol{p}}^2}{2U} a_{\gamma,\boldsymbol{p}} a_{\gamma,-\boldsymbol{p}} \right], \tag{26}$$

where we see that $a_{\gamma,\boldsymbol{p}}$ and $e_{\gamma,\boldsymbol{p}}$ are transverse modes ($\gamma = 0, 1$) describing the gauge fluctuations and dynamics of electric fluxes, respectively. The photon dispersion is defined as

$$\epsilon_{\boldsymbol{p}}^2 = 4Ug \left[3 - \frac{1}{2} \sum_{\alpha \neq \beta} \cos\left(\frac{p_\alpha}{2}\right) \cos\left(\frac{p_\beta}{2}\right) \right]$$
$$\simeq c^2 |\boldsymbol{p}|^2 + O(|\boldsymbol{p}|^4), \tag{27}$$

where $c = (Ug)^{1/2}$. This speed of emergent light, $c \simeq 0.3g$, has been estimated in simulations of the effective

ring-exchange model [17] and motivated the value of U given in Eq. (15). The Green's functions for these a and e operators can also be easily worked out. One arrives at [21]

$$G_A(\omega,\boldsymbol{p}) = \int dt e^{i\omega t}[-i\langle \mathcal{T} a_{\gamma,\boldsymbol{p}}(t) a_{\gamma,-\boldsymbol{p}}(0)\rangle], \\ = \frac{U}{\omega^2 - \epsilon_{\boldsymbol{p}}^2 + i\delta}, \tag{28a}$$

$$G_E(\omega,\boldsymbol{p}) = \int dt e^{i\omega t}[-i\langle \mathcal{T} e_{\gamma,\boldsymbol{p}}(t) e_{\gamma,-\boldsymbol{p}}(0)\rangle], \\ = \frac{\epsilon_{\boldsymbol{p}}^2}{U\left(\omega^2 - \epsilon_{\boldsymbol{p}}^2 + i\delta\right)}, \tag{28b}$$

where $\delta = 0^+$.

Finally, we have the interaction between the spinons and gauge field encapsulated in $H_{\psi A}$. This interaction can be rewritten in momentum space as

$$H_{\psi A} = -\tilde{j}_{\pm} \sum_{\mu<\nu} \sum_{\boldsymbol{x}\in\langle A\rangle} i[(\psi_{\boldsymbol{x}}^\dagger \psi_{\boldsymbol{x}+\hat{\boldsymbol{\mu}}-\hat{\boldsymbol{\nu}}} - \psi_{\boldsymbol{x}} \psi_{\boldsymbol{x}+\hat{\boldsymbol{\mu}}-\hat{\boldsymbol{\nu}}}^\dagger)(A_{\boldsymbol{x},\mu} - A_{\boldsymbol{x}+\boldsymbol{\mu}-\boldsymbol{\nu},\nu}) + (\psi_{\boldsymbol{x}+\hat{\boldsymbol{\mu}}}^\dagger \psi_{\boldsymbol{x}+\hat{\boldsymbol{\nu}}} - \psi_{\boldsymbol{x}+\hat{\boldsymbol{\nu}}}^\dagger \psi_{\boldsymbol{x}+\hat{\boldsymbol{\mu}}})(A_{\boldsymbol{x},\nu} - A_{\boldsymbol{x},\mu})], \\ \equiv -\frac{\tilde{j}_{\pm}}{\sqrt{N}} \sum_{\mu<\nu} \sum_{\boldsymbol{k}\lambda} \sum_{\rho} f^{\psi A}_{\mu\nu\rho,\lambda}(\boldsymbol{k},\boldsymbol{p}) \psi^\dagger_{\boldsymbol{k}+\boldsymbol{p},\lambda} \psi_{\boldsymbol{k}\lambda} A_{\boldsymbol{p},\rho}, \tag{29}$$

where N is the number of unit cells and we have defined the vertex

$$f^{\psi A}_{\mu\nu\rho,\lambda}(\boldsymbol{k},\boldsymbol{p}) = i\delta_{\lambda,\langle A\rangle}[\delta_{\rho\mu} e^{+i\boldsymbol{k}\cdot(\boldsymbol{\mu}-\boldsymbol{\nu})} - \delta_{\rho\nu} e^{+i(\boldsymbol{k}+\boldsymbol{p})\cdot(\boldsymbol{\mu}-\boldsymbol{\nu})} + \delta_{\rho\nu} e^{-i\boldsymbol{k}\cdot(\boldsymbol{\mu}-\boldsymbol{\nu})} - \delta_{\rho\mu} e^{-i(\boldsymbol{k}+\boldsymbol{p})\cdot(\boldsymbol{\mu}-\boldsymbol{\nu})}] \\ + i\delta_{\lambda,\langle B\rangle}[\delta_{\rho\mu} e^{+i(\boldsymbol{k}\cdot(\boldsymbol{\mu}-\boldsymbol{\nu})-\boldsymbol{p}\cdot\boldsymbol{\nu})} - \delta_{\rho\nu} e^{+i(\boldsymbol{k}\cdot(\boldsymbol{\mu}-\boldsymbol{\nu})-\boldsymbol{p}\cdot\boldsymbol{\nu})} + \delta_{\rho\nu} e^{-i(\boldsymbol{k}\cdot(\boldsymbol{\mu}-\boldsymbol{\nu})+\boldsymbol{p}\cdot\boldsymbol{\mu})} - \delta_{\rho\mu} e^{-i(\boldsymbol{k}\cdot(\boldsymbol{\mu}-\boldsymbol{\nu})+\boldsymbol{p}\cdot\boldsymbol{\mu})}]. \tag{30}$$

This part, $H_{\psi A}$, describes an interaction between the spinons ψ and the gauge field A, similar to the interaction in regular quantum electrodynamics, coupling A to the "current" of spinons. At this point, we thus have an effective theory of spinons interacting with a U(1) gauge field.

V. MICROSCOPIC ORIGIN OF THE RAMAN VERTEX

We now investigate the mechanism of light scattering from the excitations of a QSI phase. Light can interact with matter in various ways. It is well known that, in general, the strongest coupling does not come from the direct coupling of the magnetic field of the light with the magnetic moments, but rather through the coupling of its electric field to the electric dipole moments of the scattering medium [48,57]. The basic processes leading to the Raman response in Mott insulators are similar to those leading to exchange interactions, except that the virtual electron hopping is assisted by photons. Consequently, in the simplest approximation, the operator describing Raman processes is generically expected to be proportional to the spin-exchange couplings, weighted by polarization-dependent factors that determine the ability of real photons to control the magnitude of an electron hopping along certain bonds [26,27,48–50,58–60].

To describe the coupling of light to electrons on a lattice, one can, in a first approximation, perform a Peierls substitution [61], attaching a "Wilson line" operator to the electron hopping term to preserve gauge invariance [26,49,58]:

$$c_{i\sigma}^\dagger c_{j\sigma} \to c_{i\sigma}^\dagger c_{j\sigma} \exp\left[\frac{ie}{\hbar c}\int_{\boldsymbol{r}_j}^{\boldsymbol{r}_i} d\boldsymbol{r}\cdot\mathcal{A}(\boldsymbol{r})\right]. \tag{31}$$

Here, we use $\mathcal{A}$ to denote the vector potential of the radiation field, not to be confused with the emergent U(1) gauge field in QSI, which we have denoted as A. Intuitively, the photon couples to the electric dipole formed by charge transfer between different lattice sites. Thus, in order to get the correct Raman vertex, we must know the microscopic electron hopping mechanism at play in the material.

In the case of QSI, the superexchange interactions between neighboring spins are expected to be mediated by the oxygen atoms that surround each rare-earth ion [16,22] as illustrated in Fig. 1. The microscopic derivation of Eq. (1) starts from separating the total microscopic Hamiltonian into an on-site part, H_0, and the hopping between rare-earth f electrons and oxygen p electrons, V_0,

$$H = H_0 + V_0. \tag{32}$$

All other hoppings are assumed to be small and thus neglected [22]. The V_0 term is given by

$$V_0 = \sum_{\boldsymbol{x}\in\langle A\rangle} \sum_{\mu} \sum_{\alpha\beta} (t^\dagger_{\mu,\alpha\beta} p^\dagger_{\boldsymbol{x},\alpha} f_{\boldsymbol{x}\mu,\beta} + t^\dagger_{\mu,\alpha\beta} p^\dagger_{\boldsymbol{x}+\boldsymbol{\mu},\alpha} f_{\boldsymbol{x}\mu,\beta} \\ + t_{\mu,\alpha\beta} f^\dagger_{\boldsymbol{x}\mu,\beta} p_{\boldsymbol{x},\alpha} + t_{\mu,\alpha\beta} f^\dagger_{\boldsymbol{x}\mu,\beta} p_{\boldsymbol{x}+\boldsymbol{\mu},\alpha}), \tag{33}$$

where $t_{\mu,\alpha\beta}$ denotes the hopping amplitude, $f_{\boldsymbol{x}\mu,\beta}$ and $p_{\boldsymbol{x},\alpha}$ represent the electron annihilation operators on the rare-earth and oxygen ions, respectively. Here we only include the high-symmetry oxygens (Wyckoff site 8b), those which lie in the centers of the rare-earth tetrahedra, as they are closer to the rare-earth ions than the low symmetry oxygens [47]. The on-site part H_0 contains the atomic interactions of the rare-earth ion, including Coulomb, spin-orbit, and crystal field contributions. Here, we do not need the detailed properties of H_0 as long as its ground state is a doublet, and that the energy to add or remove an electron, denoted roughly as $\sim U_f$ [22], is large relative to the magnitude of the hoppings, t.

We now include the interaction with the electromagnetic (EM) field. As mentioned in Eq. (31), this coupling brings

about a modification, $V_0 \to V$, given by

$$V = \sum_{\boldsymbol{x}\in\langle A\rangle}\sum_{\mu}\sum_{\alpha\beta}\Big(t^{\dagger}_{\mu,\alpha\beta}p^{\dagger}_{\boldsymbol{x},\alpha}f_{\boldsymbol{x}\mu,\beta}e^{\frac{ie}{\hbar c}\int_{x+\frac{1}{2}\mu}^{x}d\boldsymbol{r}\cdot\mathcal{A}(\boldsymbol{r})} + t^{\dagger}_{\mu,\alpha\beta}p^{\dagger}_{\boldsymbol{x}+\boldsymbol{\mu},\alpha}f_{\boldsymbol{x}\mu,\beta}e^{\frac{ie}{\hbar c}\int_{x+\frac{1}{2}\mu}^{x+\mu}d\boldsymbol{r}\cdot\mathcal{A}(\boldsymbol{r})} + \text{H.c.}\Big). \quad (34)$$

To proceed, we make the assumption that the photon field is relatively weak, so that interaction with light does not affect the electronic structure of the material. We also assume that $\frac{ie}{\hbar c}\mathcal{A}\cdot\boldsymbol{\mu}$ is reasonably small so that we can expand V using a Taylor expansion as

$$V = V_0 + V_1 + \cdots. \quad (35)$$

Knowing that the wavelength of the incoming and outgoing EM waves is much larger than the lattice constant of the material, we can further make the replacement

$$\frac{ie}{\hbar c}\int_{\boldsymbol{x}+\frac{1}{2}\boldsymbol{\mu}}^{\boldsymbol{x}} d\boldsymbol{r}\cdot\mathcal{A}(\boldsymbol{r}) \sim -\frac{ie}{2\hbar c}(\boldsymbol{\mu}\cdot\mathcal{A}_{\boldsymbol{x}}). \quad (36)$$

Under these approximations, we have

$$V_1 = \left(\frac{ie}{2\hbar c}\right)\sum_{\boldsymbol{x}\in\langle A\rangle}\sum_{\mu,\alpha\beta}(\mathcal{A}_{\boldsymbol{x}}\cdot\boldsymbol{\mu})[t^{\dagger}_{\mu,\alpha\beta}p^{\dagger}_{\boldsymbol{x}+\boldsymbol{\mu},\alpha}f_{\boldsymbol{x}\mu,\beta} + t_{\mu,\alpha\beta}f^{\dagger}_{\boldsymbol{x}\mu,\beta}p_{\boldsymbol{x},\alpha} - t^{\dagger}_{\mu,\alpha\beta}p^{\dagger}_{\boldsymbol{x},\alpha}f_{\boldsymbol{x}\mu,\beta} - t_{\mu,\alpha\beta}f^{\dagger}_{\boldsymbol{x}\mu,\beta}p_{\boldsymbol{x}+\boldsymbol{\mu},\alpha}].$$

This differs from V_0 in that it attaches to each electron hopping term a factor $\pm\mathcal{A}\cdot\boldsymbol{\mu}$ coming from the EM field. In addition to this modification of the electron hopping, we must also now include the energy of the EM field itself, which we denote as H_γ [26].

Our goal is to derive an effective Hamiltonian, treating V as a perturbation, for the low-energy states of $H_0 + H_\gamma$. For our purposes, this low-energy subspace contains all of the relevant EM states and only the ground states of H_0. Now, from standard degenerate perturbation theory [62], this effective Hamiltonian can be written

$$H_{\text{eff}} = PH_0P + PH_\gamma P + PVP + PVRVP + PVRVRVP + PVRVRVRVP + \cdots, \quad (37)$$

in which P projects into the ground-state manifold of H_0 and R is the resolvent

$$R = \frac{1-P}{E_0 - H_0 - H_\gamma + i\delta} \approx \frac{1-P}{E_0 - H_0 + i\delta}, \quad (38)$$

where E_0 is the ground-state energy of H_0 and $\delta = 0^+$. Here, we assumed that $H_\gamma \ll H_0$, that is, the energy of the EM photon is much smaller than the atomic energy scales. We return to the effects of this approximation in Sec. VII B. The presence of the projection operator, P, implies that only even order perturbations have nonzero contribution. To get the nonresonant Raman vertex, we neglect higher-order terms in Eq. (35) and keep only V_1 as perturbation.

We now proceed to compute the effective Hamiltonian in the low-energy subspace relevant for the rare-earth ion, similar to what is done in calculations of superexchange [16,22]. Due to the structure of the superexchange processes, the anisotropic exchange Hamiltonian shown in Eq. (1) appears at fourth order [16,22] in V_0, with $H_{\text{ex}} = PV_0RV_0RV_0RV_0P$. It can be shown that the Raman interaction also comes in at fourth order in perturbation theory. To describe the scattering of light, we keep only the leading $O(\mathcal{A}^2)$ parts of H_{eff}, that is those having two factors of V_0 and two factors of V_1.[5] While second-order processes, $H_R^{(2)}$, that can contribute single-spin operators to the Raman operator do exist (see Appendix B), they vanish when only the high-symmetry oxygens are considered. We will return to this point this is Sec. VII B. To separate out the Raman part, we then can write

$$\begin{aligned} H_R^{(4)} &\equiv PVRVRVRVP - H_{\text{ex}}, \\ &= P(V_0+V_1)R(V_0+V_1)R(V_0+V_1)R(V_0+V_1)P - H_{\text{ex}}, \\ &= PV_1RV_1RV_0RV_0P + PV_1RV_0RV_1RV_0P \\ &\quad + \cdots + PV_0RV_0RV_1RV_1P. \end{aligned}$$

There are six terms that give a Raman contribution at fourth order in V, with the two V_1 terms corresponding one incoming photon and one outgoing photon, and the Raman operator can be obtained by attaching photon factors, $\sim\pm\mathcal{A}\cdot\boldsymbol{\mu}$, to two of the four hoppings in each superexchange process.

Now we can write down $H_R^{(4)}$ explicitly. We first write $\mathcal{A}_{\boldsymbol{x}}$ in terms of EM photon operators, splitting it into two parts [26,49]:

$$\mathcal{A}_{\boldsymbol{x}} \sim g_i\hat{\boldsymbol{e}}_i a_{\boldsymbol{k}_i,\hat{\boldsymbol{e}}_i}e^{i\boldsymbol{k}_i\cdot\boldsymbol{x}} + g_f\hat{\boldsymbol{e}}_f a^{\dagger}_{\boldsymbol{k}_f,\hat{\boldsymbol{e}}_f}e^{i\boldsymbol{k}_f\cdot\boldsymbol{x}} \equiv \mathcal{A}_i + \mathcal{A}_f. \quad (39)$$

Here, $a_{\boldsymbol{k}_i,\hat{\boldsymbol{e}}_i}$ and $a^{\dagger}_{\boldsymbol{k}_f,\hat{\boldsymbol{e}}_f}$ represent the real EM photons, not to be confused with the emergent excitations that exist in QSI. The vectors $\hat{\boldsymbol{e}}_i$ and $\hat{\boldsymbol{e}}_f$ denote the polarization vectors of the incoming and outgoing photons, respectively. The g_i and g_f are constant prefactors depending on the incoming/outgoing photon frequencies [26,49]. We will omit them in what follows. Further, since the photon wave vector is small relative to the inverse lattice spacing, we can safely replace $e^{i\boldsymbol{k}_i\cdot\boldsymbol{x}} \sim e^{i\boldsymbol{k}_f\cdot\boldsymbol{x}} \sim 1$, keeping only the polarization vectors $\hat{\boldsymbol{e}}_i$ and $\hat{\boldsymbol{e}}_f$.

For a hopping process involving bonds $\boldsymbol{\mu}$ and $\boldsymbol{\nu}$, the incoming and outgoing EM operator $\mathcal{A}_i$ and $\mathcal{A}_f$ can couple to $\pm\boldsymbol{\mu}$ and $\pm\boldsymbol{\nu}$. There are 12 possibilities in total for choosing two out of four bonds to couple with $\mathcal{A}_i$ and $\mathcal{A}_f$ (see Fig. 1). The overall prefactor is then found to be

$$\begin{aligned} &(\mathcal{A}_i\cdot(\pm\boldsymbol{\mu}))(\mathcal{A}_f\cdot(\mp\boldsymbol{\mu})) + (\mathcal{A}_i\cdot(\pm\boldsymbol{\mu}))(\mathcal{A}_f\cdot(\pm\boldsymbol{\nu})) \\ &\quad + (\mathcal{A}_i\cdot(\pm\boldsymbol{\mu}))(\mathcal{A}_f\cdot(\mp\boldsymbol{\nu})) + (\mu\rightleftharpoons\nu), \\ &\sim (\mathcal{A}_i\cdot\boldsymbol{\mu})(\mathcal{A}_f\cdot\boldsymbol{\mu}) + (\mathcal{A}_i\cdot\boldsymbol{\nu})(\mathcal{A}_f\cdot\boldsymbol{\nu}). \end{aligned}$$

Since the Raman vertex and the effective Hamiltonian have similar mathematical form, we can easily express the Raman vertex in terms of spin operators [26,49]. At last, the final result

[5] Note that the higher-order correction, V_2 would produce at the same order, i.e., at $O(\mathcal{A}^2)$, from the first-order perturbative contribution PV_2P. However, since V_2 still necessarily involves a charge transfer from the ligand to the rare-earth ion one has $PV_2P = 0$.

for the Raman part of the effective Hamiltonian is given by

$$H_R^{(4)} \sim \sum_{\mu<\nu}[(\mathcal{A}_i\cdot\boldsymbol{\mu})(\mathcal{A}_f\cdot\boldsymbol{\mu})+(\mathcal{A}_i\cdot\boldsymbol{\nu})(\mathcal{A}_f\cdot\boldsymbol{\nu})]\mathcal{R}_{\mu\nu}, \tag{40}$$

where the operator $\mathcal{R}_{\mu\nu}$ is defined as

$$\begin{aligned}\mathcal{R}_{\mu\nu} = \sum_{\boldsymbol{x}\in\langle A\rangle}\big[&J_{zz}\big(S^z_{\boldsymbol{x}\mu}S^z_{\boldsymbol{x}\nu}+S^z_{\boldsymbol{x}\mu}S^z_{\boldsymbol{x}+\boldsymbol{\mu}-\boldsymbol{\nu},\nu}\big)\\ &-J_{\pm}(S^+_{\boldsymbol{x}\mu}S^-_{\boldsymbol{x}\nu}+S^+_{\boldsymbol{x}\mu}S^-_{\boldsymbol{x}+\boldsymbol{\mu}-\boldsymbol{\nu},\nu}+\text{H.c.})\\ &+J_{\pm\pm}(\gamma_{\mu\nu}(S^+_{\boldsymbol{x}\mu}S^+_{\boldsymbol{x}\nu}+S^+_{\boldsymbol{x}\mu}S^+_{\boldsymbol{x}+\boldsymbol{\mu}-\boldsymbol{\nu},\nu})+\text{H.c.})\\ &+J_{z\pm}(\zeta_{\mu\nu}S^z_{\boldsymbol{x}\mu}(S^+_{\boldsymbol{x}\nu}+S^+_{\boldsymbol{x}+\boldsymbol{\mu}-\boldsymbol{\nu},\nu})+\text{H.c.}+(\mu\rightleftharpoons\nu))\big].\end{aligned} \tag{41}$$

This gives the full nonresonant Raman vertex, $\mathcal{R}$, for incoming light with polarization $\hat{\boldsymbol{e}}_i$ scattered to light with polarization $\hat{\boldsymbol{e}}_f$ as

$$\mathcal{R}\equiv\sum_{\mu<\nu}[(\hat{\boldsymbol{e}}_i\cdot\boldsymbol{\mu})(\hat{\boldsymbol{e}}_f\cdot\boldsymbol{\mu})+(\hat{\boldsymbol{e}}_i\cdot\boldsymbol{\nu})(\hat{\boldsymbol{e}}_f\cdot\boldsymbol{\nu})]\mathcal{R}_{\mu\nu}. \tag{42}$$

Using the definition of the lattice vectors $\boldsymbol{\mu}$ (see Appendix A), the Raman vertex can be rewritten as

$$\mathcal{R}=\frac{1}{8}\hat{\boldsymbol{e}}_i\cdot\begin{pmatrix}\sum_{\mu<\nu}\mathcal{R}_{\mu\nu} & \mathcal{R}_{03}-\mathcal{R}_{12} & \mathcal{R}_{02}-\mathcal{R}_{13}\\ \mathcal{R}_{03}-\mathcal{R}_{12} & \sum_{\mu<\nu}\mathcal{R}_{\mu\nu} & \mathcal{R}_{01}-\mathcal{R}_{23}\\ \mathcal{R}_{02}-\mathcal{R}_{13} & \mathcal{R}_{01}-\mathcal{R}_{23} & \sum_{\mu<\nu}\mathcal{R}_{\mu\nu}\end{pmatrix}\cdot\hat{\boldsymbol{e}}_f. \tag{43}$$

We see that the vertex naturally breaks into two channels corresponding to the irreducible representations A_{1g} and T_{2g} of the point group O_h of the pyrochlore lattice. The fully symmetric A_{1g} operator is given by

$$\mathcal{R}_{A_{1g}}\equiv\sum_{\mu<\nu}\mathcal{R}_{\mu\nu}=\mathcal{R}_{01}+\mathcal{R}_{02}+\mathcal{R}_{03}+\mathcal{R}_{12}+\mathcal{R}_{13}+\mathcal{R}_{23}, \tag{44}$$

while the three components of the T_{2g} channels are given by

$$\mathcal{R}_{T^x_{2g}}\equiv\mathcal{R}_{01}-\mathcal{R}_{23}, \tag{45a}$$

$$\mathcal{R}_{T^y_{2g}}\equiv\mathcal{R}_{02}-\mathcal{R}_{13}, \tag{45b}$$

$$\mathcal{R}_{T^z_{2g}}\equiv\mathcal{R}_{03}-\mathcal{R}_{12}. \tag{45c}$$

At this level of approximation, the Raman vertex in the A_{1g} channel is proportional to the Hamiltonian (1) and, thus, does not induce any inelastic transitions. Therefore, in what follows, we focus on the T_{2g} channel, which is the only active Raman channel in the QSI within the approach developed here (see Sec. VII B for a discussion of some limitations). More compactly, dropping the $\mathcal{R}_{A_{1g}}$ operator, the effective Raman operator $\mathcal{R}$ is then

$$\mathcal{R}\sim\sum_{\alpha\beta\gamma}|\epsilon_{\alpha\beta\gamma}|\big(\hat{e}_i^{\alpha}\hat{e}_f^{\beta}+\hat{e}_i^{\beta}\hat{e}_f^{\alpha}\big)\mathcal{R}_{T^{\gamma}_{2g}}, \tag{46}$$

where $\epsilon_{\alpha\beta\gamma}$ is the Levi-Cevita symbol. We next outline how to compute the Raman response in the T_{2g} channel.

VI. RAMAN RESPONSE IN QUANTUM SPIN ICE

We now compute the Raman scattering intensity at energy transfer $\Omega\equiv\omega_i-\omega_f$ using Fermi's golden rule, which is proportional to

$$\mathcal{I}(\Omega)\equiv\sum_n|\langle n|\mathcal{R}|0\rangle|^2\delta(\Omega-E_n+E_0), \tag{47}$$

where $\mathcal{R}$ is the Raman operator given by Eq. (46) and E_n, $|n\rangle$ are the energies and eigenstates of the system. Also, since we are interested the Raman response at zero temperature we only have intensity for positive Ω. It is convenient to compute the Raman response using the time-ordered Raman response function

$$F(\Omega)\equiv\int dt\, e^{i\Omega t}[-i\langle\mathcal{T}\mathcal{R}(t)\,\mathcal{R}(0)\rangle], \tag{48}$$

where $\langle\cdots\rangle$ is the average is with respect to the ground state. In the spectral representation, $F(\Omega)$ can be written as

$$F(\Omega)\equiv\sum_n\left[\frac{|\langle n|\mathcal{R}|0\rangle|^2}{\Omega-E_n+E_0+i\delta}-\frac{|\langle n|\mathcal{R}|0\rangle|^2}{\Omega+E_n-E_0-i\delta}\right], \tag{49}$$

where $\delta=0^+$. We then simply have that the intensity is given by

$$\mathcal{I}(\Omega)=\frac{1}{\pi}\Theta(\Omega)\,\mathrm{Im}F(\Omega), \tag{50}$$

where $\Theta(\Omega)$ is the Heaviside function. It is convenient to define a generalized response tensor

$$\mathcal{D}_{\mu\nu,\mu'\nu'}(t)=-i\langle\mathcal{T}\mathcal{R}_{\mu\nu}(t)\mathcal{R}_{\mu'\nu'}(0)\rangle \tag{51}$$

from which we can assemble the physical intensity of interest. Similarly, we can define a generalized intensity

$$\mathcal{I}_{\mu\nu,\mu'\nu'}(\Omega)=\frac{1}{\pi}\Theta(\Omega)\mathrm{Im}\left[\int dt\, e^{i\Omega t}\mathcal{D}_{\mu\nu,\mu'\nu'}(t)\right]. \tag{52}$$

For example, in terms of this generalized intensity, the response in the T^x_{2g} channel is given by

$$\mathcal{I}_{T^x_{2g}}(\Omega)\equiv\mathcal{I}_{01,01}(\Omega)-\mathcal{I}_{01,23}(\Omega)-\mathcal{I}_{23,01}(\Omega)+\mathcal{I}_{23,23}(\Omega). \tag{53}$$

Since the QSI state is fully symmetric, the intensity in each of the T^{α}_{2g} channels is identical. We thus use a common notation $\mathcal{I}_{T^x_{2g}}=\mathcal{I}_{T^y_{2g}}=\mathcal{I}_{T^z_{2g}}\equiv\mathcal{I}_{T_{2g}}$.

To aid in the interpretation of these results, we divide the Raman operators and the intensities into several parts that represent qualitatively distinct physical processes. As for the H_{QSI} Hamiltonian in Eq. (16), we can write the Raman operator in terms of the spinons and gauge fields. We thus write the generalized Raman operator, $\mathcal{R}_{\mu\nu}$, as a sum of several contributions:

$$\mathcal{R}_{\mu\nu}\equiv\mathcal{R}^{\psi}_{\mu\nu}+\mathcal{R}^{\psi A}_{\mu\nu}+\mathcal{R}^{E}_{\mu\nu}. \tag{54}$$

There are three parts here: the scattering from spinons, $\mathcal{R}^{\psi}$, the scattering from a combination of spinon and gauge excitations, $\mathcal{R}^{\psi A}$, and the scattering from the emergent light itself, $\mathcal{R}^{E}$. In computing the Raman operator, we consider only the leading terms of the exponential of the gauge field, as we

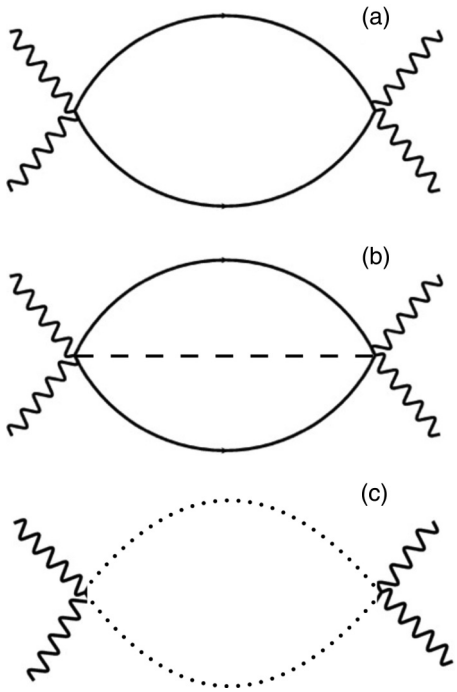

FIG. 2. Three classes of diagrams needed for calculating the Raman scattering intensity from various QSI excitations: (a) spinon excitations, (b) coupled spinon and gauge-field excitations, and (c) e excitations. Solid, dashed, and dotted lines represent $G_\psi(\omega,\boldsymbol{k})$, $G_A(\omega,\boldsymbol{p})$, and $G_E(\omega,\boldsymbol{p})$ propagators for the spinons, the a and the e fields, respectively. The wavy lines correspond to the incoming and outgoing photons.

did in Eq. (16). The $\mathcal{R}^{\psi}_{\mu\nu}$ and $\mathcal{R}^{\psi A}_{\mu\nu}$ are closely related to the decomposition of $H_{\rm QSI}$ [Eq. (16)] into H_ψ and $H_{\psi A}$. Schematically, the Feynman diagrams for contributions to the Raman intensity from the scattering from spinons, from a combination of spinon and gauge excitations, and the scattering from the emergent light are shown in Fig. 2.

We begin with the terms in the Raman operator of Eq. (41) proportional to $J_\pm$ which can be written as spinon-only and spinon-gauge interactions. These terms can be expressed analogously to H_ψ and $H_{\psi A}$ [see Eqs. (17) and (29)] as

$$\mathcal{R}^{\psi}_{\mu\nu} = -\tilde{j}_\pm \sum_{\boldsymbol{k}\lambda} f^{\psi}_{\mu\nu}(\boldsymbol{k})\psi^\dagger_{\boldsymbol{k}\lambda}\psi_{\boldsymbol{k}\lambda}, \tag{55a}$$

$$\mathcal{R}^{\psi A}_{\mu\nu} = -\frac{\tilde{j}_\pm}{\sqrt{N}} \sum_{\boldsymbol{k}\boldsymbol{p}\lambda}\sum_{\rho} f^{\psi A}_{\mu\nu\rho,\lambda}(\boldsymbol{k},\boldsymbol{p})\psi^\dagger_{\boldsymbol{k}+\boldsymbol{p},\lambda}\psi_{\boldsymbol{k}\lambda}A_{\boldsymbol{p},\rho}, \tag{55b}$$

where the vertex $f^{\psi}_{\mu\nu}(\boldsymbol{k})$ is defined in Eq. (18) and the vertex $f^{\psi A}_{\mu\nu\rho,\lambda}(\boldsymbol{k},\boldsymbol{p})$ is defined in Eq. (30).

Next, we consider the terms of the Raman operator [Eq. (41)] that are proportional to J_{zz}. These terms can be written using the electric field operators $E_{\boldsymbol{x}\mu}$ as

$$\begin{aligned}\mathcal{R}^{E}_{\mu\nu} &\equiv \sum_{\boldsymbol{x}\in\langle A\rangle}(E_{\boldsymbol{x}\mu}E_{\boldsymbol{x}\nu} + E_{\boldsymbol{x}\mu}E_{\boldsymbol{x}+\boldsymbol{\mu}-\boldsymbol{\nu},\nu}),\\ &= \sum_{\boldsymbol{k}} f^{\mu\nu}_{E}(\boldsymbol{k})E_{\boldsymbol{k},\mu}E_{-\boldsymbol{k},\nu},\end{aligned} \tag{55c}$$

where we have defined the vertex

$$f^{E}_{\mu\nu}(\boldsymbol{k}) \equiv 1 + e^{-i\boldsymbol{k}\cdot(\boldsymbol{\mu}-\boldsymbol{\nu})}. \tag{56}$$

Note that, in contrast to the J_{zz} parts of the Hamiltonian, since the Raman operator contains $\sim \sum_{\boldsymbol{x}} S^z_{\boldsymbol{x}\mu}S^z_{\boldsymbol{x}\nu}$, not summed over μ,ν, one cannot easily represent this operator in terms of the charges $Q_{\boldsymbol{x}}$.

At leading order, the three parts of Eq. (54) do not mix since they create distinct sets of excitations. We now calculate the intensity for each of these different mechanisms.

A. Spinon-only contribution

This process involves the light scattering from a pair of spinons. Since the incoming light carries (essentially) zero momentum, this pair of particles must also have zero total momentum. The spinon-only part of the response tensor is given by

$$\begin{aligned}\mathcal{D}^{\psi}_{\mu\nu,\mu'\nu'}(t) &\equiv -i\langle\mathcal{T}\mathcal{R}^{\psi}_{\mu\nu}(t)\mathcal{R}^{\psi}_{\mu'\nu'}\rangle, \qquad (57)\\ &= -i\,\tilde{j}^2_\pm \sum_{\boldsymbol{k}\lambda,\boldsymbol{k}'\lambda'} f^{\psi}_{\mu\nu}(\boldsymbol{k})f^{\psi}_{\mu'\nu'}(\boldsymbol{k}'),\\ &\quad\times\langle\mathcal{T}\psi^\dagger_{\boldsymbol{k}\lambda}(t)\psi_{\boldsymbol{k}\lambda}(t)\psi^\dagger_{\boldsymbol{k}'\lambda'}\psi_{\boldsymbol{k}'\lambda'}\rangle, \qquad (58)\end{aligned}$$

where $\mathcal{R}^{\psi}_{\mu\nu}$ is defined in Eq. (55a) and $f^{\psi}_{\mu\nu}(\boldsymbol{k})$ in Eq. (18). Using Eq. (22), we can write the response tensor as

$$\mathcal{D}^{\psi}_{\mu\nu,\mu'\nu'}(t) = 2i\,\tilde{j}^2_\pm \sum_{\boldsymbol{k}} f^{\psi}_{\mu\nu}(\boldsymbol{k})f^{\psi}_{\mu'\nu'}(\boldsymbol{k})G_\psi(\boldsymbol{k},t)G_\psi(\boldsymbol{k},t), \tag{59}$$

where $G_\psi(\boldsymbol{k},t)$ is the Green's function of the spinon in real time. The product of vertices $f^{\psi}_{\mu\nu}(\boldsymbol{k})$ can be simplified to

$$f^{\psi}_{\mu\nu}(\boldsymbol{k})f^{\psi}_{\mu'\nu'}(\boldsymbol{k}) = 4\cos[\boldsymbol{k}\cdot(\boldsymbol{\mu}-\boldsymbol{\nu})]\cos[\boldsymbol{k}\cdot(\boldsymbol{\mu}'-\boldsymbol{\nu}')]. \tag{60}$$

The intensity tensor for the spinon-only contribution is thus given by

$$\begin{aligned}\mathcal{I}^{\psi}_{\mu\nu,\mu'\nu'}(\Omega) &\equiv \frac{1}{\pi}\Theta(\Omega)\,\mathrm{Im}\int dt\; e^{i\Omega t}\mathcal{D}^{S}_{\mu\nu,\mu'\nu'}(t),\\ &= 2\tilde{j}^2_\pm \sum_{\boldsymbol{k}} \frac{f^{\psi}_{\mu\nu}(\boldsymbol{k})f^{\psi}_{\mu'\nu'}(\boldsymbol{k})}{4E^2_{\boldsymbol{k}}}\delta(\Omega-2E_{\boldsymbol{k}}),\end{aligned} \tag{61}$$

where the Green's function integrals are computed using conventional techniques [63]. To obtain the response in the T_{2g} channel, we use Eq. (53) and find

$$\begin{aligned}\mathcal{I}^{\psi}_{T_{2g}}(\Omega) &= \tilde{j}^2_\pm \sum_{\boldsymbol{k}} \frac{8}{E^2_{\boldsymbol{k}}}\sin^2\left(\frac{k_y}{2}\right)\sin^2\left(\frac{k_z}{2}\right)\delta(\Omega-2E_{\boldsymbol{k}})\\ &= \tilde{j}^2_\pm \sum_{\boldsymbol{k}} \frac{8}{E^2_{\boldsymbol{k}}}\left[\frac{1}{3}\sum_{\alpha<\beta}\sin^2\left(\frac{k_\alpha}{2}\right)\sin^2\left(\frac{k_\beta}{2}\right)\right]\\ &\quad\times\delta(\Omega-2E_{\boldsymbol{k}}).\end{aligned} \tag{62}$$

In the last step, we have symmetrized the vertex to emphasize that this intensity is the same for each of the $\mathcal{R}_{T^\alpha_{2g}}$ Raman operators.

B. Spinon-gauge contribution

Next, we consider the spinon-gauge contribution. Here, in addition to exciting a spinon-pair, the light also excites an emergent photon. Due to the accompanying emergent photon, the spinon-pair can now have arbitrary total momentum. To evaluate the intensity, we consider the response tensor

$$\mathcal{D}^{\psi A}_{\mu\nu,\mu'\nu'}(t) = -i\langle \mathcal{T}\mathcal{R}^{\psi A}_{\mu\nu}(t)\mathcal{R}^{\psi A}_{\mu'\nu'}(0)\rangle, \tag{63}$$

where $\mathcal{R}^{\psi A}_{\mu\nu}$ is defined in Eq. (55b). The next step in computing $\mathcal{D}^{\psi A}_{\mu\nu,\mu'\nu'}(t)$ is the evaluation of

$$-i\langle \mathcal{T}\psi^{\dagger}_{\boldsymbol{k}+\boldsymbol{p},\lambda}(t)\psi_{\boldsymbol{k}\lambda}(t)A_{\boldsymbol{p},\rho}(t)\psi^{\dagger}_{\boldsymbol{k}'+\boldsymbol{p}',\lambda'}\psi_{\boldsymbol{k}'\lambda'}A_{\boldsymbol{p}',\rho'}\rangle.$$

There is one nonvanishing contraction, which yields

$$-\delta_{\boldsymbol{p},-\boldsymbol{p}'}\delta_{\boldsymbol{k}',\boldsymbol{k}+\boldsymbol{p}}\delta_{\boldsymbol{k},\boldsymbol{k}'+\boldsymbol{p}'}\delta_{\lambda\lambda'}\delta_{\rho\rho'}G_{\psi}(\boldsymbol{k},t)G_{\psi}(\boldsymbol{k}+\boldsymbol{p},t)G_{A}(\boldsymbol{p},t), \tag{64}$$

where $G_{\psi}(\boldsymbol{k},t)$ and $G_A(\boldsymbol{p},t)$ are the Green's function of the spinon and gauge field, respectively, as defined in Eqs. (22) and (28a). The response tensor $\mathcal{D}^{\psi A}_{\mu\nu,\mu'\nu'}(t)$ is then given by

$$-\frac{\tilde{j}_{\pm}^2}{N}\sum_{\boldsymbol{k}\boldsymbol{p}}\Phi_{\mu\nu,\mu'\nu'}(\boldsymbol{k},\boldsymbol{p})G_{\psi}(\boldsymbol{k},t)G_{\psi}(\boldsymbol{k}+\boldsymbol{p},t)G_{A}(\boldsymbol{p},t),$$

where we have defined the vertex

$$\Phi_{\mu\nu,\mu'\nu'}(\boldsymbol{k},\boldsymbol{p}) = \sum_{\lambda\rho}\left[f^{\psi A}_{\mu\nu\rho,\lambda}(\boldsymbol{k},\boldsymbol{p})\right]^{*} f^{\psi A}_{\mu'\nu'\rho,\lambda}(\boldsymbol{k},\boldsymbol{p}).$$

Performing the time integral [see Eq. (52)] using standard contour methods, we obtain the intensity tensor in the spinon and gauge-field channel to be

$$\mathcal{I}^{\psi A}_{\mu\nu,\mu'\nu'}(\Omega) = \frac{\tilde{j}_{\pm}^2}{N}\sum_{\boldsymbol{k}\boldsymbol{p}}\Phi_{\mu\nu,\mu'\nu'}(\boldsymbol{k},\boldsymbol{p})\frac{U}{8E_{\boldsymbol{k}}E_{\boldsymbol{k}+\boldsymbol{p}}\epsilon_{\boldsymbol{p}}} \times \delta(\Omega-(E_{\boldsymbol{k}}+E_{\boldsymbol{k}+\boldsymbol{p}}+\epsilon_{\boldsymbol{p}})). \tag{65}$$

For the T_{2g} channel, the vertex is given by

$$\Phi_{T_{2g}}(\boldsymbol{k},\boldsymbol{p}) = 16\left[1-\cos\left(k_y+\frac{p_y}{2}\right)\cos\left(k_z+\frac{p_z}{2}\right)\right]. \tag{66}$$

The final result for the spinon-gauge contribution to the T_{2g} intensity is then

$$\mathcal{I}^{\psi A}_{T_{2g}}(\Omega) = \frac{\tilde{j}_{\pm}^2}{N}\sum_{\boldsymbol{k}\boldsymbol{p}}\frac{2U}{E_{\boldsymbol{k}}E_{\boldsymbol{k}+\boldsymbol{p}}\epsilon_{\boldsymbol{p}}}\delta(\Omega-(E_{\boldsymbol{k}}+E_{\boldsymbol{k}+\boldsymbol{p}}+\epsilon_{\boldsymbol{p}})) \times\left[1-\cos\left(k_y+\frac{p_y}{2}\right)\cos\left(k_z+\frac{p_z}{2}\right)\right].$$

We see that if the photon energy scale is small, the intensity is proportional to the density of states of the spinon pairs with arbitrary total momentum. As for the spinon-only case, we rewrite the intensity $\mathcal{I}^{\psi A}_{T_{2g}}(\Omega)$ in a manifestly symmetric form as

$$\mathcal{I}^{\psi A}_{T_{2g}}(\Omega) = \frac{\tilde{j}_{\pm}^2}{N}\sum_{\boldsymbol{k}\boldsymbol{p}}\frac{2U}{E_{\boldsymbol{k}}E_{\boldsymbol{k}+\boldsymbol{p}}\epsilon_{\boldsymbol{p}}}\delta(\Omega-(E_{\boldsymbol{k}}+E_{\boldsymbol{k}+\boldsymbol{p}}+\epsilon_{\boldsymbol{p}})) \times\left[1-\frac{1}{3}\sum_{\alpha<\beta}\cos\left(k_\alpha+\frac{p_\alpha}{2}\right)\cos\left(k_\beta+\frac{p_\beta}{2}\right)\right].$$

C. Electric field contribution

Finally, we consider the contribution from the electric field alone. Physically, this process corresponds to the light exciting a pair of emergent photons. As in the case of spinons alone, the pair of emergent photons has zero total momentum. The relevant response tensor is

$$\begin{aligned}\mathcal{D}^{E}_{\mu\nu,\mu'\nu'}(t) &\equiv -i\langle \mathcal{T}\mathcal{R}^{E}_{\mu\nu}(t)\mathcal{R}^{E}_{\mu'\nu'}\rangle \\ &= \sum_{\boldsymbol{p}\boldsymbol{p}'} f_E^{\mu\nu}(\boldsymbol{p})f_E^{\mu'\nu'}(\boldsymbol{p}') \\ &\quad\times[-i\langle \mathcal{T}E_{\boldsymbol{p}\mu}(t)E_{-\boldsymbol{p}\nu}(t)E_{\boldsymbol{p}'\mu'}E_{-\boldsymbol{p}'\nu'}\rangle],\end{aligned} \tag{67}$$

where $\mathcal{R}^{E}_{\mu\nu}$ is defined in Eq. (55c). This correlation function has two relevant contractions leading to

$$\mathcal{D}^{E}_{\mu\nu,\mu'\nu'}(t) = i\sum_{\boldsymbol{p}}[\delta_{\mu\nu'}\delta_{\mu'\nu}+\delta_{\mu\mu'}\delta_{\nu\nu'}]\left|f_E^{\mu\nu}(\boldsymbol{p})\right|^2 G_E(\boldsymbol{p},t)^2,$$

where the Green's function for the electric field, $G_E(\boldsymbol{k},t)$, is defined in Eq. (28b). Evaluating the time integral [see Eq. (52)], one finds

$$\begin{aligned}&\frac{1}{\pi}\mathrm{Im}\int dt\, e^{i\Omega t}iG_E(\boldsymbol{p},t)^2 \\ &\quad= \frac{\epsilon_{\boldsymbol{p}}^2}{4U^2}[\delta(\Omega+2\epsilon_{\boldsymbol{p}})+\delta(\Omega-2\epsilon_{\boldsymbol{p}})].\end{aligned}$$

We thus have the generalized intensity from the electric fields

$$\begin{aligned}&\mathcal{I}^{E}_{\mu\nu,\mu'\nu'}(\Omega) \\ &\quad= \sum_{\boldsymbol{p}}\frac{\epsilon_{\boldsymbol{p}}^2}{4U^2}[\delta_{\mu\nu'}\delta_{\mu'\nu}+\delta_{\mu\mu'}\delta_{\nu\nu'}]\left|f_E^{\mu\nu}(\boldsymbol{p})\right|^2\delta(\Omega-2\epsilon_{\boldsymbol{p}}).\end{aligned}$$

The intensity can easily be evaluated for the T_{2g} channel, yielding

$$\begin{aligned}\mathcal{I}^{E}_{T_{2g}}(\Omega) &= \sum_{\boldsymbol{p}}\frac{\epsilon_{\boldsymbol{p}}^2}{U^2}\left[1+\cos\left(\frac{p_y}{2}\right)\cos\left(\frac{p_z}{2}\right)\right]\delta(\Omega-2\epsilon_{\boldsymbol{p}}) \\ &= \sum_{\boldsymbol{p}}\frac{\epsilon_{\boldsymbol{p}}^2}{U^2}\left[1+\frac{1}{3}\sum_{\alpha<\beta}\cos\left(\frac{p_\alpha}{2}\right)\cos\left(\frac{p_\beta}{2}\right)\right] \\ &\quad\times\delta(\Omega-2\epsilon_{\boldsymbol{p}}).\end{aligned} \tag{68}$$

This intensity reflects the density of states of a pair of emergent photons with total momentum zero. Again, as in the spinon-only and spinon-gauge cases, we have written the symmetric form for this intensity.

D. Total intensity

The total intensity in the T_{2g} channel is thus given by the following sum:

$$\mathcal{I}_{T_{2g}}(\Omega) = \mathcal{I}^{\psi}_{T_{2g}}(\Omega)+\mathcal{I}^{\psi A}_{T_{2g}}(\Omega)+\mathcal{I}^{E}_{T_{2g}}(\Omega), \tag{69}$$

where the three different contributions are given by

$$\mathcal{I}^{\psi}_{T_{2g}}(\Omega) = \tilde{j}_{\pm}^2 \sum_{\boldsymbol{k}} \frac{8}{E_{\boldsymbol{k}}^2}\left[\frac{1}{3}\sum_{\alpha<\beta}\sin^2\left(\frac{k_\alpha}{2}\right)\sin^2\left(\frac{k_\beta}{2}\right)\right]\delta(\Omega - 2E_{\boldsymbol{k}}), \tag{70a}$$

$$\mathcal{I}^{\psi A}_{T_{2g}}(\Omega) = \tilde{j}_{\pm}^2 \sum_{\boldsymbol{k}} \left\{\frac{1}{N}\sum_{\boldsymbol{p}} \frac{2U}{E_{\boldsymbol{k}} E_{\boldsymbol{k}+\boldsymbol{p}} \epsilon_{\boldsymbol{p}}}\left[1 - \frac{1}{3}\sum_{\alpha<\beta}\cos\left(k_\alpha + \frac{p_\alpha}{2}\right)\cos\left(k_\beta + \frac{p_\beta}{2}\right)\right]\delta(\Omega - (E_{\boldsymbol{k}} + E_{\boldsymbol{k}+\boldsymbol{p}} + \epsilon_{\boldsymbol{p}}))\right\}, \tag{70b}$$

$$\mathcal{I}^{E}_{T_{2g}}(\Omega) = \sum_{\boldsymbol{p}} \frac{\epsilon_{\boldsymbol{p}}^2}{U^2}\left[1 + \frac{1}{3}\sum_{\alpha<\beta}\cos\left(\frac{p_\alpha}{2}\right)\cos\left(\frac{p_\beta}{2}\right)\right]\delta(\Omega - 2\epsilon_{\boldsymbol{p}}). \tag{70c}$$

A brief comment is in order. We see that when $\tilde{j}_{\pm} = 0$, i.e., when the underlying system is simply a classical spin ice, the contributions from the coupled spinon and gauge fields and from spinons alone both explicitly vanish, $\mathcal{I}^{\psi A}_{T_{2g}} = 0$ and $\mathcal{I}^{\psi}_{T_{2g}} = 0$. The intensity $\mathcal{I}^{E}_{T_{2g}}$ from the electric part of the gauge field comes from the J_{zz} term and does not have explicit proportionality to $\tilde{j}_{\pm}$. Nevertheless, this contribution also vanishes when $\tilde{j}_{\pm} = 0$; without the quantum tunneling terms, a spin Hamiltonian containing only J_{zz} terms commutes with the Raman operator and, therefore, does not lead to a Raman response. More explicitly, the photon dispersion collapses as $\tilde{j}_{\pm} \to 0$, since $\epsilon_{\boldsymbol{p}} \propto \tilde{j}_{\pm}^3$, leading to the zero response at nonzero frequency shift Ω.

E. Numerical results

With the developed formalism in hand, we now numerically evaluate the Raman intensities in the T_{2g} polarization channel. We examine the contribution from each of the different physical processes: namely the spinon-only, spinon-gauge, and gauge-only contributions. The single sums found in Eqs. (70a) and (70b) were evaluated on a grid of 384^3 $\boldsymbol{k}$ points, with the origin shifted by a small amount to resolve any singularities in the vertices at $\boldsymbol{k} = 0$. For the double sum of Eq. (70c), a similar procedure was employed, but 48^3 points for each momentum proved sufficient to reach convergence. The results for the Raman intensity profiles are presented in Fig. 3. This figure contains the main results of this paper. All intensities are computed assuming $j_{\pm} = 0.05$ (taking $\langle s^{\pm}\rangle = 1$ for simplicity) and are normalized to the maximum intensity of the spinon-only Raman response.

First, we consider the Raman intensity from the spinon-only scattering. As expected, this contribution has intensity centered around the classical spinon energy cost $\sim J_{zz}$ with a width proportional to the energy of the tunneling term $J_{\pm}$. Since the incoming light can only generate a spinon pair with zero total momentum, this channel does not probe the full two-spinon continuum. Some aspects of the spinon-only response can be better understood by considering the zero-momentum, two-spinon density of states defined as

$$\rho_{\psi}(\Omega) \propto \sum_{\boldsymbol{k}} \delta(\Omega - 2E_{\boldsymbol{k}}), \tag{71}$$

as shown in Fig. 4(a). Here we see that the onset of the spinon density of states is $\sim\sqrt{\Omega - \Omega_0}$ with $\Omega_0 = \sqrt{1 - 12\tilde{j}_{\pm}}$ being twice the gap in the spinon dispersion of Eq. (21). Further, the density of states also has a sharp peak (Van Hove singularity) due to the presence of flat regions in the spinon dispersion [21]. These features—a slow onset at low frequencies and a large intensity near the maximum of the two-spinon band—are characteristic features of the two-spinon Raman response.

The Raman response from coupled spinon and gauge fluctuations also takes the form of a broad continuum in roughly the same range of energies as the two-spinon case. However, the excitation of the emergent gauge photon now allows access to the full two-spinon continuum, as its presence relaxes the constraint on having zero total momentum for the spinon pair. While this does not change the maximum or minimum of the two-spinon energies (compared to the zero-momentum case), it does affect the intensity profile at intermediate energies. As in the spinon-only case, the spinon-gauge intensity can be better understood by considering the corresponding density of states

$$\rho_{\psi A}(\Omega) \propto \sum_{\boldsymbol{k}\boldsymbol{p}} \delta(\Omega - (E_{\boldsymbol{k}} + E_{\boldsymbol{k}+\boldsymbol{p}} + \epsilon_{\boldsymbol{p}})), \tag{72}$$

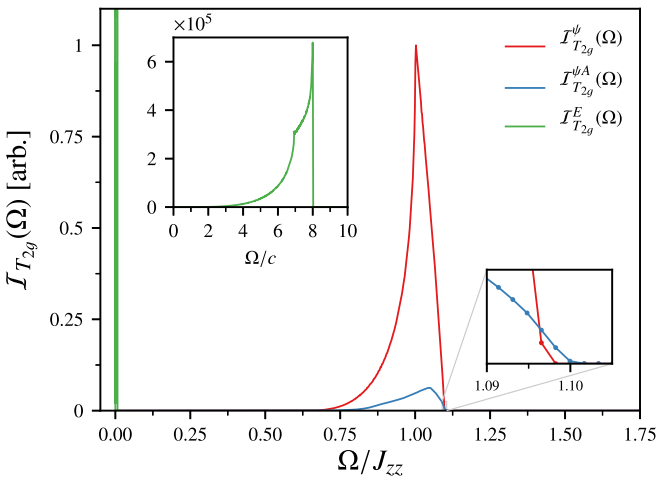

FIG. 3. The Raman intensities in the T_{2g} polarization channel computed for QSI. Contributions from the pure spinon contribution (blue line), from the coupled spinon and gauge fluctuations (red line), and from the gauge fluctuations coming from the E field (green line) are shown, as defined in Eq. (70). All intensities are normalized on the maximum intensity of the spinon-only Raman response, when taken alone.

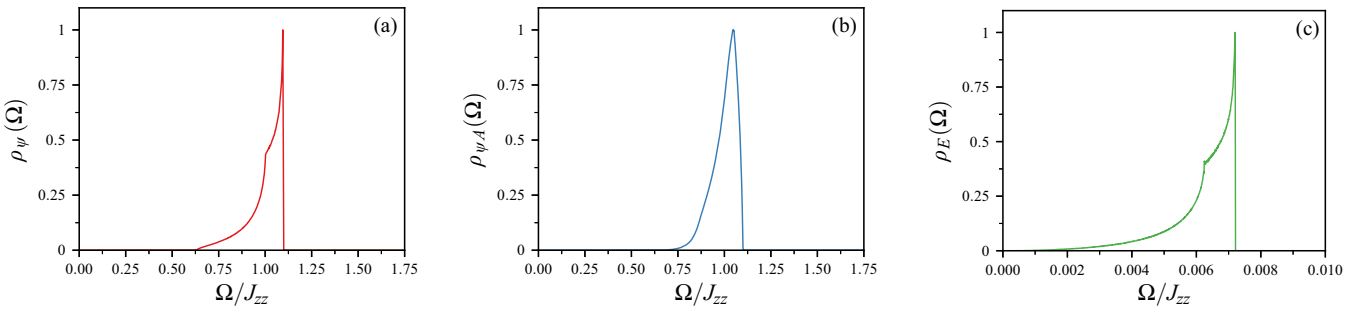

FIG. 4. Density of states for (a) zero-momentum two-spinon states [see Eq. (71)], (b) two-spinon states and an emergent photon [see Eq. (72)], and (c) two emergent photons alone [see Eq. (73)]. Each density of states is normalized arbitrarily, such that its own individual maximum value is equal to one.

as shown in Fig. 4(b). One important feature to note is that the width of this broad continuum is slightly larger than that of the pure two-spinon scattering; due to the interaction with the gauge-field, the combined spinon-photon states can reach higher energies than the spinons alone. This can be seen in the bottom right inset of Fig. 3, where the upper edge of the intensity is pushed to higher energies. However, this shift is quite small, being proportional to the emergent photon bandwidth, which scales as $\sim j_\pm^3$. Given this fact, we can effectively ignore the energy of gauge particle in the δ functions in $\mathcal{I}_{T_{2g}}^{\psi A}$. Physically, the photon is thus acting as a "momentum sink" for the spinon pair: for essentially zero energy cost one can excite a photon with arbitrary momentum.

Finally, we consider the gauge-field-only response from the emergent electric field. It appears as a strong, sharp peak at the energies corresponding to the emergent photon bandwidth. The energy scale of the emergent photon dispersion relation goes as $\sim j_\pm^3$ and is thus much smaller than the energy scale of the aforementioned features that involve the spinons. The intensity profile of the Raman response in this case follows very closely the zero-momentum, two-photon density of states

$$\rho_E(\Omega) \propto \sum_{\boldsymbol{p}} \delta(\Omega - 2\epsilon_{\boldsymbol{p}}), \tag{73}$$

which is shown in Fig. 4(c). At low energies, this intensity follows a power law $\sim\Omega^2$ due to the linear photon dispersion. The flat dispersion in the photon band structure at the edge of the band (at $\Omega = 8c$) is also apparent high intensity at the highest energies. The larger intensity relative to the spinon features seen in Fig. 3 originates from the lack of a $\sim j_\pm^2$ prefactor in the Raman intensity since this scattering processes is due to the large J_{zz} interactions, and the narrow support in Ω. Even with this narrow support in energy, the overall energy-integrated scattering is significantly stronger from the photon sector than from the spinon sector, as can be seen directly from Eqs. (70a)–(70c).

VII. DISCUSSION

In this section, we discuss some of the limitations of the results derived in this work and how they may affect applications to real materials. In particular, we discuss the microscopic origins of the Raman operator, the approximations made in the slave-particle formulation and speculate on the effects of the so far ignored anisotropic $J_{\pm\pm}$ and $J_{z\pm}$ interactions on the Raman intensity.

A. Slave-particle formulation

In Secs. III and IV, we introduced a slave-particle formulation for QSI and a framework to enable calculation of the Raman response. There are a number of approximations involved in the slave-particle framework used in this work.

First, in our analysis, we considered only the first-order coupling between the spinons and gauge fluctuations, i.e., we kept only the first order terms in the expansion of the exponential e^{iA}. This approximation is not necessarily controlled. Indeed this approximation removes completely the gauge monopoles [14], a set of excitations of the gauge sector with energy comparable to that of the emergent photon. These excitations appear only nonperturbatively in A. A detailed analysis of corrections from the higher orders in the expansion of e^{iA} gauge sector and the possibility of including the gauge monopoles are left for future exploration.

Second, we have computed the response for the XXZ model where only $j_\pm$ is nonzero. The features seen in the intensities are likely to be modified if the Raman response was computed for the complete and more general anisotropic exchange model, Eq. (1) [18,19]. The $J_{z\pm}$ terms would bring another spinon-gauge field interaction vertex, and the $J_{\pm\pm}$ terms would bring a four-spinon interaction vertex. A detailed analysis of these vertices is, technically, significantly more involved, and we therefore leave it for future study. However, we believe that the basic qualitative features of the Raman response, the broad intensity continuum and its width would not be changed significantly by the inclusion of these interactions.[6] On the other hand, the detailed features, such as the sharpness of the peak in the spinon-only response, would likely be modified.

Third, one key deficiency in the mean-field theory presented in Sec. III is that the effects of the gauge-field on the spinon are treated in an averaged way. It is unclear whether such an approximation is valid in QSI, given the energy scale of the photon is much lower than the kinetic energy of the spinons

[6]Note that a pure $J_{\pm\pm}$ coupling, with $J_\pm = J_{z\pm} = 0$ would not produce spinon pairs, but two singly charged spinons and one doubly charged spinon. Therefore, in this case, the intensity would appear only near the much higher energy $3J_{zz}$.

[64]. However, recent more exact treatments of the spinon excitations in related contexts [64–66], which have found that treating the spinon as a (strongly) renormalized free particle [64,65], may not be too poor of an approximation.

Finally, we note that the emergent photon-only response is derived entirely from the gauge part of the model, H_g. This is essentially equivalent to the lattice gauge theory of Ref. [17] used to describe the physics of QSI when the spinons are not included. This description has proven to be quite accurate in computing the static properties of QSI in this limit, faithfully reproducing the results of direct simulation [17]. We thus expect that our results for the low energy, electric only part of the Raman intensity to be robust, as it is independent of some of these coarser approximations used in the slave-particle formulation.

B. Microscopic considerations

In Sec. V, we derived the Raman operator through degenerate perturbation theory. In doing so we made several approximations that simplify both the calculation and the final form of the Raman operator.

First, we comment on the generated polarization channels. Within the approximations used, one obtains an inactive A_{1g} channel and an active T_{2g} channel. The Raman operator $\mathcal{R}$ [see Eq. (41)] for each of these channels mimics closely the "parent" exchange model, $H_{\rm ex}$ [see Eq. (1)], with the different anisotropic interactions appearing in the same ratios as in the exchange Hamiltonian. The appearance of these exchange constants in the Raman operator is predicated on the assumption that one can neglect the photon energies in the resolvent denominators in the perturbation theory. When this condition is relaxed, the form of the Raman operator becomes decoupled from that of the exchange Hamiltonian. Indeed, the rich structure of the intermediate states involved in rare-earth superexchange processes [67] will likely affect not only the scale of the interactions, but also the relative importance of the various anisotropic terms. Because of this, we would expect additional polarization channels to be generated and that the inactive A_{1g} would become active. Roughly, such corrections would be proportional to ω_i/U_f where ω_i is the incoming light frequency and U_f is a typical rare-earth charge-transfer energy scale.

Second, we note here that our treatment of the Raman intensity only includes contributions from two-ion processes, whereas single-ion processes have not been included in our calculation. Since the energy cost of single-spin flips and two-spin-flips can be of the same order in QSI materials, these processes might also be important. This can be contrasted with the separation of energy scale in one- and two-magnon processes in conventionally ordered magnets [48]. For Kramers ions, any single-ion Raman operator is necessarily time-reversal odd, and thus must vanish as the frequency of the incoming light becomes small relative to the atomic energy scales [68], providing some suppression of such contributions. Further, the Raman response will be nonzero only in the T_{1g} channel, as time-reversal odd operators only appear in anti-symmetric channels, which for O_h there is only T_{1g} [68]. For non-Kramers ion, the single-ion transverse $S^{\pm}$ operators can appear in the Raman operator without such suppression. Within the context of our calculations here, such single-ion terms are most easily generated via second-order virtual processes that only involve oxygen atoms that are not in the centers of tetrahedra, so-called axial oxygens. For the two axial oxygens we have included (see Fig. 1 and Sec. V), such a contribution vanishes (for details see Appendix B). However, there are six additional, lower symmetry oxygens that we have not considered [47]. If these are included, single-ion terms are generated and they contribute to the Raman response in both the E_g and T_{2g} channels. However, these may be somewhat suppressed given the larger distance to these oxygens [47]. Even given these complications, one should note that these single-ion operators probe the same excitations as the two-ion operators; the $S^{\pm}$ type terms excite spinon pairs, while the S^z type terms excite emergent photons. We thus do not expect any qualitative change in the results presented here for the T_{2g} channel when such single-ion terms are included.

VIII. CONCLUSIONS

In this paper, we proposed a theory of the Raman scattering in the XXZ limit of the general anisotropic exchange model, which we analyzed using a slave-particle formulation of QSI [21]. We derived the Raman vertex using the traditional framework of an effective Hamiltonian for the interaction of light with spin degrees of freedom [26,48–50]. We showed that, at fourth order in perturbation theory, the Raman vertex of Eq. (42) takes a Loudon-Fleury form [48], generated by photon-assisted superexchange, following the anisotropic exchange model [Eq. (16)] that leads to the QSI behavior. We also showed that the Raman vertex naturally decomposes into two channels corresponding to the irreducible representations A_{1g} and T_{2g} of the lattice point group. Moreover, since the Raman vertex in the A_{1g} channel commutes with the QSI Hamiltonian, the Raman intensity is nonzero only in the T_{2g} polarization channel. Within this framework, we decomposed the Raman intensity into three contributions, from the pure spinon field, coupled spinon and gauge fluctuations and the emergent photon. We showed that the dominant feature of the overall response consists of a broad continuum from the two-spinon spectrum and a sharp narrow peak at low energy originating from the gauge fluctuations of the emergent photon field taken alone. To conclude, we comment below on a few general aspects of Raman scattering as well as discuss relevance of our results to real candidate QSI materials.

First, a unique feature of Raman scattering is the ability to probe characteristics of a system that are not directly related to the magnetic moments. For example, the QSI candidates to date have mostly been studied with tools such as neutron scattering [4]. While this approach has proven to be very powerful, there are some limitations when the pseudospins are of dipolar-octupolar or non-Kramers character, as they are in $Dy_2Ti_2O_7$, $Ho_2Ti_2O_7$, $Tb_2Ti_2O_7$, and in the $Pr_2M_2O_7$ family. For these compounds, the transverse components of the pseudo-spin are higher multipoles (quadrupoles or octupoles) and thus are not easily visible in neutron scattering. So while inelastic neutron scattering could observe the photon excitation in such materials (in principle, with sufficient energy resolution) [17], observing the spinon excitations is very

difficult.[7] The possibility of seeing the two-spinon continuum at all, irrespective of resolving distinct signatures or features, is from a fundamental perspective a strong asset for Raman scattering as a probe of QSI candidate materials.

Second, from a broader perspective, we would like to comment on the possibility to use Raman scattering as a tool to study the phase transitions between different magnetic phases. In particular, it would be interesting to compare the Raman responses arising from a QSL phase and nearby ordinary magnetically ordered phase appearing at slightly different set of parameters of the same model. For example, aside from exotic phases such as QSI and the conjectured Coulomb ferromagnet [19], there are also four magnetically ordered phases found in the phase diagram of the anisotropic exchange model. These are the antiferromagnetic Γ_5 states, a family of splayed ferromagnets, the Palmer-Chalker state and the all-in/all-out (AIAO) order [21,69]. Even in the simple limit considered here with $j_{\pm\pm} = j_{z\pm} = 0$, there is the nearby Γ_5 state that is stabilized for $j_\pm \gtrsim 0.06$ [42,44]. The transition into the state can be captured with the slave-particle description used here and it corresponds to the condensation of the spinons [19,22], which is similar to the gauge symmetry breaking in the Higgs' mechanism. More generally, near the boundary of a QSL and a magnetically ordered phase, one may expect both the conventional excitations of the ordered phases and the unconventional excitations of the QSL to be generically present. Whether the spinon-gauge-field formalism can still be productively applied within the ordered antiferromagnetic phase remains an open question. If it is possible, one may be able to compute the Raman response for the antiferromagnetic phase using the same description as the one used for the QSI and then, the Raman response may be used as a tool to study the phase transition between these two phases. In general, in frustrated magnetic systems, both the response from the QSL and from the magnetically ordered state will have a broad Raman intensity background with some peak structure [27–30,59,60]. Thus, in order to understand the origin of the broad continua in the Raman spectrum, one needs to identify the nature of the excitations, disentangle the contributions of individual quasiparticles with different energies, and make a detailed, quantitative comparison between theory and experiment. In all, this is not a trivial question to answer and detailed discussion on this issue is still lacking.

One last and yet very important question to address is the possibility to see the Raman responses in experiments on real QSI materials. As far as we know, no magnetic Raman experiments have been done on QSI materials so far. One clear obstacle is the fact that the energy scale of exchange interactions in rare-earth magnets is considerably smaller than one in many transitional metal magnets. For the rare-earth pyrochlore quantum spin ice materials, these coupling constants are typically on the order of 0.1 meV. Coupling constants of this magnitude will produce the gross features (scattering from spinons) at energies of order 1–2 cm^{-1}, which is, unfortunately, much smaller than the lower limit accessible by current Raman spectroscopy, which typically probes excitations ranging 1–100 meV (10–1000 cm^{-1}) [58]. However, one possible way to resolve this conundrum might be with Brillouin scattering, which does well for probing energy scales 0.01–1 meV (0.1–10 cm^{-1}) [57,70] and which differs from Raman scattering technique only by the type of spectrometer. However, even with such a setup, the intensity due to scattering from the emergent photon is likely to remain challenging to expose. Indeed, even with the improved energy resolution afforded by a Brillouin scattering setup, the photon contribution to the intensity is likely to be difficult to distinguish from any elastic scattering in the T_{2g} channel. One could potentially infer the presence of the photon contribution through temperature dependence of the quasielastic response. The results here apply for temperatures much smaller than the photon energy scale g; as the temperature is raised this will be enhanced until it crosses over to the purely elastic response expected for classical spin ice. Further complications can arise in spin ice systems where the spin ice manifold itself is split by dipolar interactions, such as in $Dy_2Ti_2O_7$ or $Ho_2Ti_2O_7$. This splitting carries over to the spinon (or classical "monopole") excitations [41] and thus could mimic the effects of a quantum dispersion in the Raman intensity.

On the other hand, as material science is a fast developing field of research, we believe that new QSI materials with stronger quantum effects may be designed or discovered. One tantalizing possibility could be the discovery of a transition-metal quantum spin ice candidate. If such a system were to exist, a large increase (one or two orders of magnitude) in energy scale relative to the rare-earth materials considered in the present work could possibly render many of the features discussed here at much more experimentally accessible energies. In such a scenario, not only the spinon continuum, but the emergent photon itself could even be visible within experimentally accessible energy ranges.

ACKNOWLEDGMENTS

The authors are grateful to Girsh Blumberg, Kenneth Burch, Zhihao Hao, and Brent Perreault for helpful discussions. N. P. and J. F. acknowledge the support from NSF DMR-1511768 Grant. N. P. and J.F. are thankful to the Perimeter Institute for hospitality during the course of this work. Research at the Perimeter Institute is supported by the Government of Canada through Industry Canada and by the Province of Ontario through the Ministry of Economic Development and Innovation. Part of this work was also performed at the Aspen Center for Physics, which is supported by NSF Grant No. PHY-1066293. The work at the University of Waterloo was supported by the Natural Sciences and Engineering Research Council of Canada (NSERC), the Canada Research Chair (CRC) program (M.J.P.G., Tier 1) and the Canadian Institute for Advanced Research (CIfAR).

[7]For the case of dipolar-octupolar doublets [51], there are some possible routes around this restriction. In this case both S^z and S^x transform as dipoles oriented along the local $\hat{z}$ direction and thus can mix. In principle, the exchange interactions could stabilize a spin ice in a mixed direction, i.e., $\sum_{\langle ij\rangle} \tilde{S}_i^z \tilde{S}_j^z$, where $\tilde{S}_i^z = S_i^z \cos\theta + S_i^x \sin\theta$. In this case, the moment operator, $\propto S^z$, then involves both $\tilde{S}^z$ and $\tilde{S}^x$ and thus can probe the spinon excitations. The spinon excitations would also be visible in the so-called "octupolar" QSI introduced in Ref. [51]. In $Dy_2Ti_2O_7$, the interactions between the dipoles is dominant and any mixing is thought to be minimal [22].

APPENDIX A: THE DEFINITION OF LOCAL COORDINATE SPACE AND THE ζ MATRIX

The definition of the lattice vectors $\boldsymbol{\mu}$ is

$$\hat{\mathbf{0}} = \frac{+\hat{\boldsymbol{x}} + \hat{\boldsymbol{y}} + \hat{\boldsymbol{z}}}{4}, \quad \hat{\mathbf{1}} = \frac{+\hat{\boldsymbol{x}} - \hat{\boldsymbol{y}} - \hat{\boldsymbol{z}}}{4},$$
$$\hat{\mathbf{2}} = \frac{-\hat{\boldsymbol{x}} + \hat{\boldsymbol{y}} - \hat{\boldsymbol{z}}}{4}, \quad \hat{\mathbf{3}} = \frac{-\hat{\boldsymbol{x}} - \hat{\boldsymbol{y}} + \hat{\boldsymbol{z}}}{4}, \tag{A1}$$

where $\hat{\boldsymbol{x}}, \hat{\boldsymbol{y}}, \hat{\boldsymbol{z}}$ denote the global cubic axes. The local coordinates $(\hat{\boldsymbol{x}}_\mu, \hat{\boldsymbol{y}}_\mu, \hat{\boldsymbol{z}}_\mu)$ for the four sites (labeled as $\mu = 0,1,2,3$) of a certain tetrahedron of the pyrochlore lattice are defined as

$$\hat{\boldsymbol{x}}_0 = \frac{-2\hat{\boldsymbol{x}} + \hat{\boldsymbol{y}} + \hat{\boldsymbol{z}}}{\sqrt{6}}, \hat{\boldsymbol{y}}_0 = \frac{-\hat{\boldsymbol{y}} + \hat{\boldsymbol{z}}}{\sqrt{2}}, \hat{\boldsymbol{z}}_0 = \frac{+\hat{\boldsymbol{x}} + \hat{\boldsymbol{y}} + \hat{\boldsymbol{z}}}{\sqrt{3}}, \tag{A2a}$$

$$\hat{\boldsymbol{x}}_1 = \frac{-2\hat{\boldsymbol{x}} - \hat{\boldsymbol{y}} - \hat{\boldsymbol{z}}}{\sqrt{6}}, \hat{\boldsymbol{y}}_1 = \frac{+\hat{\boldsymbol{y}} - \hat{\boldsymbol{z}}}{\sqrt{2}}, \hat{\boldsymbol{z}}_1 = \frac{+\hat{\boldsymbol{x}} - \hat{\boldsymbol{y}} - \hat{\boldsymbol{z}}}{\sqrt{3}}, \tag{A2b}$$

$$\hat{\boldsymbol{x}}_2 = \frac{+2\hat{\boldsymbol{x}} + \hat{\boldsymbol{y}} - \hat{\boldsymbol{z}}}{\sqrt{6}}, \hat{\boldsymbol{y}}_2 = \frac{-\hat{\boldsymbol{y}} - \hat{\boldsymbol{z}}}{\sqrt{2}}, \hat{\boldsymbol{z}}_2 = \frac{-\hat{\boldsymbol{x}} + \hat{\boldsymbol{y}} - \hat{\boldsymbol{z}}}{\sqrt{3}}, \tag{A2c}$$

$$\hat{\boldsymbol{x}}_3 = \frac{+2\hat{\boldsymbol{x}} - \hat{\boldsymbol{y}} + \hat{\boldsymbol{z}}}{\sqrt{6}}, \hat{\boldsymbol{y}}_3 = \frac{+\hat{\boldsymbol{y}} + \hat{\boldsymbol{z}}}{\sqrt{2}}, \hat{\boldsymbol{z}}_3 = \frac{-\hat{\boldsymbol{x}} - \hat{\boldsymbol{y}} + \hat{\boldsymbol{z}}}{\sqrt{3}}. \tag{A2d}$$

In Eq. (1), the phase factors γ and ζ are defined as [18,19]

$$\gamma_{\mu\nu} = \begin{pmatrix} 0 & 1 & \omega & \omega^2 \\ 1 & 0 & \omega^2 & \omega \\ \omega & \omega^2 & 0 & 1 \\ \omega^2 & \omega & 1 & 0 \end{pmatrix}_{\mu\nu}, \tag{A3}$$

where $\omega = e^{2\pi i/3}$ and $\zeta_{\mu\nu} = -\gamma^*_{\mu\nu}$.

APPENDIX B: SECOND-ORDER CONTRIBUTIONS TO THE RAMAN VERTEX

Here we consider the second-order terms, $\sim PVRVP$, in the perturbative expansion Eq. (37). These processes can only result in operators acting on a single rare-earth ion. Evaluating these terms within the charging approximation [16,22], one finds

$$H_R^{(2)} = PV_1RV_1P,$$
$$\sim -\left(\frac{e}{\hbar c}\right)^2 \sum_{\alpha\beta\mu} (\hat{\boldsymbol{e}}_i \cdot \boldsymbol{\mu})(\hat{\boldsymbol{e}}_f \cdot \boldsymbol{\mu}) \frac{2[t_\mu t_\mu^\dagger]^{\alpha\beta}}{U_f}$$
$$\times \sum_{\boldsymbol{x}\in\langle A\rangle} P f_{\boldsymbol{x}\mu,\beta} f^\dagger_{\boldsymbol{x}\mu,\alpha} P, \tag{B1}$$

where, loosely, U_f is an energy scale associated with the cost transferring a hole from an oxygen to the rare-earth ion. As in Sec. V, we include only hoppings to the high-symmetry oxygens [47] that sit at the centers of the rare-earth tetrahedra (Wyckoff site 8*b*). By construction, $H_R^{(2)}$ is symmetric in the polarizations $\hat{\boldsymbol{e}}_i$ and $\hat{\boldsymbol{e}}_f$. Since coupling to time-reversal odd operators must be in antisymmetric channels [68], no time-reversal odd operators can be generated by this process. The absence of time-reversal odd operators holds even when the charging approximation [22] is lifted and when energy of the light is included in the resolvents. For Kramers doublets, this implies that $H_R^{(2)}$ does not contribute to the Raman response. For non-Kramers doublets, this implies any operators appearing $H_R^{(2)}$ must be time-reversal even. We can thus (effectively) consider the operator

$$P f_{\boldsymbol{x}\mu,\beta} f^\dagger_{\boldsymbol{x}\mu,\alpha} P \sim h^0_{\beta\alpha} + h^+_{\beta\alpha} S^-_{\boldsymbol{x}\mu} + h^-_{\beta\alpha} S^+_{\boldsymbol{x}\mu}. \tag{B2}$$

For a given rare-earth site, the two high-symmetry oxygens are along the local [111] directions, i.e., $\pm\hat{\boldsymbol{z}}$. Because of this, within the Slater-Koster (two-center) approximation [71], one then has that $t_\mu t_\mu^\dagger$ is diagonal. The diagonal operators $P f_{\boldsymbol{x}\mu,\alpha} f^\dagger_{\boldsymbol{x}\mu,\alpha} P$ are then invariant under rotations about the $\hat{\boldsymbol{z}}_\mu$. Since the $S^\pm_{\boldsymbol{x}\mu}$ are not invariant under these rotations, this implies that $h^\pm_{\alpha\beta} = 0$. Note that this argument precluding the appearance of the $S^\pm_{\boldsymbol{x}\mu}$ operators holds even when the charging approximation is lifted and when the energy of the light is included, since the resolvents are invariant under threefold rotations about $\hat{\boldsymbol{z}}_\mu$. We thus see that, within our approximations, when only these two high symmetry oxygens [47] are included there is no second order, or single-ion, contributions to the Raman response.

Note that this result, i.e., that lack of single-ion terms in non-Kramers ions, does *not* follow when the low-symmetry oxygens [47] (Wyckoff site 48*f*) are included, and thus generically one has $h^\pm_{\alpha\beta} \neq 0$. In addition, inclusion of additional hoppings in t_μ, beyond the Slater-Koster approximation, would render $t_\mu t_\mu^\dagger$ non-diagonal and thus also give $h^\pm_{\alpha\beta} \neq 0$. We thus expect that for non-Kramers ions one can have single-ion response from such operators.

[1] P. Anderson, Mater. Res. Bull. **8**, 153 (1973).
[2] X.-G. Wen, Phys. Rev. B **65**, 165113 (2002).
[3] L. Balents, Nature (London) **464**, 199 (2010).
[4] M. J. P. Gingras and P. A. McClarty, Rep. Prog. Phys. **77**, 056501 (2014).
[5] L. Savary and L. Balents, Rep. Prog. Phys. **80**, 016502 (2017).
[6] S. Yan, D. A. Huse, and S. R. White, Science **332**, 1173 (2011).
[7] S. Depenbrock, I. P. McCulloch, and U. Schollwöck, Phys. Rev. Lett. **109**, 067201 (2012).
[8] T.-H. Han, J. S. Helton, S. Chu, D. G. Nocera, J. A. Rodriguez-Rivera, C. Broholm, and Y. S. Lee, Nature (London) **492**, 406 (2012).
[9] Y. Iqbal, F. Becca, S. Sorella, and D. Poilblanc, Phys. Rev. B **87**, 060405 (2013).

[10] I. Rousochatzakis, Y. Wan, O. Tchernyshyov, and F. Mila, Phys. Rev. B **90**, 100406 (2014).
[11] A. Kitaev, Ann. Phys. **321**, 2 (2006).
[12] S. Mandal and N. Surendran, Phys. Rev. B **79**, 024426 (2009).
[13] M. Hermanns, K. O'Brien, and S. Trebst, Phys. Rev. Lett. **114**, 157202 (2015).
[14] M. Hermele, M. P. A. Fisher, and L. Balents, Phys. Rev. B **69**, 064404 (2004).
[15] H. R. Molavian, M. J. P. Gingras, and B. Canals, Phys. Rev. Lett. **98**, 157204 (2007).
[16] S. Onoda and Y. Tanaka, Phys. Rev. B **83**, 094411 (2011).
[17] O. Benton, O. Sikora, and N. Shannon, Phys. Rev. B **86**, 075154 (2012).
[18] K. A. Ross, L. Savary, B. D. Gaulin, and L. Balents, Phys. Rev. X **1**, 021002 (2011).
[19] L. Savary and L. Balents, Phys. Rev. Lett. **108**, 037202 (2012).
[20] S. B. Lee, S. Onoda, and L. Balents, Phys. Rev. B **86**, 104412 (2012).
[21] Z. Hao, A. G. R. Day, and M. J. P. Gingras, Phys. Rev. B **90**, 214430 (2014).
[22] J. G. Rau and M. J. P. Gingras, Phys. Rev. B **92**, 144417 (2015).
[23] C. Wang and T. Senthil, Phys. Rev. X **6**, 011034 (2016).
[24] L. Savary, X. Wang, H.-Y. Kee, Y. B. Kim, Y. Yu, and G. Chen, Phys. Rev. B **94**, 075146 (2016).
[25] J. Knolle, D. L. Kovrizhin, J. T. Chalker, and R. Moessner, Phys. Rev. B **92**, 115127 (2015).
[26] W.-H. Ko, Z.-X. Liu, T.-K. Ng, and P. A. Lee, Phys. Rev. B **81**, 024414 (2010).
[27] J. Knolle, G.-W. Chern, D. L. Kovrizhin, R. Moessner, and N. B. Perkins, Phys. Rev. Lett. **113**, 187201 (2014).
[28] B. Perreault, J. Knolle, N. B. Perkins, and F. J. Burnell, Phys. Rev. B **92**, 094439 (2015).
[29] B. Perreault, J. Knolle, N. B. Perkins, and F. J. Burnell, Phys. Rev. B **94**, 060408 (2016).
[30] B. Perreault, J. Knolle, N. B. Perkins, and F. J. Burnell, Phys. Rev. B **94**, 104427 (2016).
[31] W.-H. Ko and P. A. Lee, Phys. Rev. B **84**, 125102 (2011).
[32] G. B. Halász, N. B. Perkins, and J. van den Brink, Phys. Rev. Lett. **117**, 127203 (2016).
[33] L. Savary and T. Senthil, arXiv:1506.04752.
[34] D. Wulferding, P. Lemmens, P. Scheib, J. Röder, P. Mendels, S. Chu, T. Han, and Y. S. Lee, Phys. Rev. B **82**, 144412 (2010).
[35] L. J. Sandilands, Y. Tian, K. W. Plumb, Y.-J. Kim, and K. S. Burch, Phys. Rev. Lett. **114**, 147201 (2015).
[36] L. J. Sandilands, Y. Tian, A. A. Reijnders, H.-S. Kim, K. W. Plumb, Y.-J. Kim, H.-Y. Kee, and K. S. Burch, Phys. Rev. B **93**, 075144 (2016).
[37] S. Nath Gupta, P. V. Sriluckshmy, K. Mehlawat, A. Balodhi, D. K. Mishra, S. R. Hassan, T. V. Ramakrishnan, D. V. S. Muthu, Y. Singh, and A. K. Sood, Eur. Phys. Lett. **114**, 47004 (2016).
[38] A. Glamazda, P. Lemmens, S.-H. Do, Y. S. Choi, and K.-Y. Choi, Nat. Commun. **7**, 12286 (2016).
[39] S. N. Gupta, P. V. Sriluckshmy, A. Balodhi, D. V. S. Muthu, S. R. Hassan, Y. Singh, T. V. Ramakrishnan, and A. K. Sood, Phys. Rev. B **94**, 155153 (2016).
[40] S. T. Bramwell and M. J. Gingras, Science **294**, 1495 (2001).
[41] C. Castelnovo, R. Moessner, and S. L. Sondhi, Nature (London) **451**, 42 (2008).
[42] A. Banerjee, S. V. Isakov, K. Damle, and Y. B. Kim, Phys. Rev. Lett. **100**, 047208 (2008).
[43] N. Shannon, O. Sikora, F. Pollmann, K. Penc, and P. Fulde, Phys. Rev. Lett. **108**, 067204 (2012).
[44] Y. Kato and S. Onoda, Phys. Rev. Lett. **115**, 077202 (2015).
[45] P. A. McClarty, O. Sikora, R. Moessner, K. Penc, F. Pollmann, and N. Shannon, Phys. Rev. B **92**, 094418 (2015).
[46] M. Kwasigroch, B. Douçot, and C. Castelnovo, Phys. Rev. B **95**, 134439 (2017).
[47] J. S. Gardner, M. J. P. Gingras, and J. E. Greedan, Rev. Mod. Phys. **82**, 53 (2010).
[48] P. A. Fleury and R. Loudon, Phys. Rev. **166**, 514 (1968).
[49] B. S. Shastry and B. I. Shraiman, Phys. Rev. Lett. **65**, 1068 (1990).
[50] B. S. Shastry and B. I. Shraiman, Int. J. Mod. Phys. B **05**, 365 (1991).
[51] Y.-P. Huang, G. Chen, and M. Hermele, Phys. Rev. Lett. **112**, 167203 (2014).
[52] L. Savary, K. A. Ross, B. D. Gaulin, J. P. C. Ruff, and L. Balents, Phys. Rev. Lett. **109**, 167201 (2012).
[53] M. E. Zhitomirsky, M. V. Gvozdikova, P. C. W. Holdsworth, and R. Moessner, Phys. Rev. Lett. **109**, 077204 (2012).
[54] J. Robert, E. Lhotel, G. Remenyi, S. Sahling, I. Mirebeau, C. Decorse, B. Canals, and S. Petit, Phys. Rev. B **92**, 064425 (2015).
[55] H. Takatsu, S. Onoda, S. Kittaka, A. Kasahara, Y. Kono, T. Sakakibara, Y. Kato, B. Fåk, J. Ollivier, J. W. Lynn, T. Taniguchi, M. Wakita, and H. Kadowaki, Phys. Rev. Lett. **116**, 217201 (2016).
[56] J. B. Kogut, Rev. Mod. Phys. **51**, 659 (1979).
[57] W. Hayes and R. Loudon, *Scattering of Light by Crystals* (Courier Corporation, Dover Publications, Inc. Mineola, New York, 2012).
[58] T. P. Devereaux and R. Hackl, Rev. Mod. Phys. **79**, 175 (2007).
[59] N. Perkins and W. Brenig, Phys. Rev. B **77**, 174412 (2008).
[60] N. B. Perkins, G.-W. Chern, and W. Brenig, Phys. Rev. B **87**, 174423 (2013).
[61] D. R. Hofstadter, Phys. Rev. B **14**, 2239 (1976).
[62] I. Lindgren, J. Phys. B: At. Mol. Phys. **7**, 2441 (1974).
[63] G. D. Mahan, *Many Particle Physics*, 3rd ed. (Kluwer Academic/ Plenum Publishers, New York, 2000).
[64] Y. Wan, J. Carrasquilla, and R. G. Melko, Phys. Rev. Lett. **116**, 167202 (2016).
[65] S. Kourtis and C. Castelnovo, Phys. Rev. B **94**, 104401 (2016).
[66] O. Petrova, R. Moessner, and S. L. Sondhi, Phys. Rev. B **92**, 100401 (2015).
[67] N. Iwahara and L. F. Chibotaru, Phys. Rev. B **91**, 174438 (2015).
[68] T. Moriya, J. Appl. Phys. **39**, 1042 (1968).
[69] H. Yan, O. Benton, L. Jaubert, and N. Shannon, Phys. Rev. B **95**, 094422 (2017).
[70] A. Polian, J. Raman Spectrosc. **34**, 633 (2003).
[71] J. C. Slater and G. F. Koster, Phys. Rev. **94**, 1498 (1954).